AER/AGS Report 97

Alberta Energy Regulator

Measurements of the States of In Situ Stress for the Duvernay Formation near Fox Creek, West-Central Alberta

AGS
ALBERTA GEOLOGICAL SURVEY

AER/AGS Report 97

Measurements of the States of In Situ Stress for the Duvernay Formation near Fox Creek, West-Central Alberta

L. Shen[1,2], D.R. Schmitt[2,3] and K. Haug[1]

[1] Alberta Energy Regulator
Alberta Geological Survey
[2] Department of Physics, University of Alberta
[3] Department of Earth, Atmospheric, and Planetary Science, Purdue University

October 2018

ISBN 978-1-4601-3977-6

Shen, L., Schmitt, D.R., and Haug, K. (2018): Measurements of the states of in situ stress for the Duvernay Formation near Fox Creek, west-central Alberta; Alberta Energy Regulator / Alberta Geological Survey, AER/AGS Report 97, 29 p.

Author addresses:
L. Shen
Department of Physics
University of Alberta
Edmonton, AB
T6G 2E3 Canada
Tel: 780.427.0015
Email: luyi@ualberta.ca
D.R. Schmitt
Department of Earth, Atmospheric, and Planetary Science
Purdue University
West Lafayette, IN 47907
United States
Tel: 765.775.8227
Email: schmitt@purdue.edu

Published October 2018 by:
Alberta Energy Regulator
Alberta Geological Survey
4th Floor, Twin Atria Building
4999 – 98th Avenue
Edmonton, AB
T6B 2X3 Canada

Tel: 780.638.4491
Fax: 780.422.1459
Email: AGS-Info@aer.ca
Website: www.ags.aer.ca

Contents

Figures

Acknowledgements

We thank AER/AGS for the permission to develop and publish this work. D.R. Schmitt is supported by the Natural Sciences and Engineering Research Council of Canada (NSERC) Research Chair Program.

Abstract

Maps of the in situ stress directions and magnitudes at the depth of the Duvernay Formation within the Alberta Energy Regulator's Kaybob assessment area, centred on the town of Fox Creek, Alberta, were constructed from multiple sets of oriented borehole images, density logs, and static and dynamic wellbore-pressure tests collected from nearby boreholes that targeted the Duvernay Formation. Azimuths of borehole breakouts and drilling-induced tensile fractures interpreted from borehole image logs reveal that the orientation of maximum horizontal compressive stress (S_H) in the Kaybob assessment area is dominantly northeast-southwest, mainly in agreement with the typical stress directions throughout much of the Alberta Basin. Vertical-stress magnitudes (S_V) come from estimates of the overburden pressures obtained by integration of more than 1000 smoothed density logs (more than 600 of which fall within the Kaybob assessment area), indicating stress to depth ratios of between 24 and 26 kPa/m for the Duvernay Formation at depths ranging between 2800 and 4000 m in the area near Fox Creek.

Dynamic borehole-pressurization tests, variously referred to as minifrac, microfrac, and diagnostic fluid-injection tests (DFITs), were reanalyzed. A consistent procedure is adapted to find the fracture-closure pressure (P_{FC}), which is here taken to be equal to the minimum horizontal compression (S_h). The closure pressure was measured as ~60 MPa at 2800 m depth, increasing to ~85 MPa at 3800 m. Minimum stress to depth ratio is constrained to between ~17 and ~22 kPa/m for the study area. Pore pressures (P_P) were also estimated from the pressurization tests. The computed average pore pressure for the Duvernay Formation near Fox Creek is estimated at ~55 MPa (2800 m) to ~80 MPa (3800 m). The pore pressure to depth ratio ranges from ~10 to ~21 kPa/m and demonstrates considerable overpressure.

1 Introduction

In the last decade, the combination of advanced horizontal drilling and hydraulic-stimulation methods in unconventional reservoirs has significantly affected North American hydrocarbon production. Understanding the states of stress at depth in the subsurface is critical to the development of these low-permeability unconventional resources and the assessment of their associated geological hazards. The state of stress is the crucial factor affecting the efficacy and safety of hydraulic fracturing, as it controls not only the pressure required to create and propagate fractures, but also their size and propagation direction. This understanding has motivated efforts to better quantitatively assess the magnitudes and orientations of the stress tensor, the pore-fluid pressures, and the rock-mass strength.

The Duvernay Formation of Alberta (Figure 1) has shown particular promise as an unconventional reservoir for light hydrocarbons (Rokosh et al., 2012) and is an active target for drilling and hydraulic-fracture stimulation near the town of Fox Creek, Alberta. The Kaybob assessment area (Preston et al., 2016), which includes the Kaybob South Field and Fox Creek Field (Green and Mountjoy, 2005) within the Duvernay Shale oil/gas play, has seen the most hydraulic-fracturing activities. This area is of further interest because hydraulic-fracture stimulations have been linked with induced seismic events (Atkinson et al., 2016; Wang et al., 2016; Schultz et al., 2017). To adequately assess the susceptibility of this area to geological hazards (Pawley et al., 2018) associated with hydraulic fracturing, it is vital that the state of stress is quantitatively understood as thoroughly as possible.

This report presents our effort in collecting and analyzing the measurements conducted by the industry to constrain the stress magnitudes, directions, and pore pressures. The dataset presented in this study comprises mainly the interpretation of borehole image logs and pressure records collected at depth near the Duvernay Formation in Alberta. Maps were compiled, with the collected data, for the regions within a portion of the Kaybob assessment area. We also reviewed the knowledge of stresses in the area and, more generally, within the Western Canada Sedimentary Basin (WCSB) prior to this study. The methods employed to obtain stress information from the various datasets are described. The data collected during this study are provided as a tabular digital dataset (Shen et al., 2018).

2 Stress States of Earth's Upper Crust

2.1 Definitions

At sufficient depths in a sedimentary basin with gently varying topography, it is commonly assumed that one of the principal components of the stress tensor is vertical with magnitude equal to the overburden pressure. This vertically directed principal stress is denoted S_V. Under this assumption, the directions of the two other orthogonal principal stresses must then lie in the horizontal plane and are called the maximum (S_H) and minimum (S_h) horizontal stress. Additionally, if we express the state of stress using the Cauchy stress tensor (σ), there must exist at least one orthogonal coordinate system in which the full tensor of the stresses can be expressed as

$$\sigma = \begin{bmatrix} S_H & 0 & 0 \\ 0 & S_h & 0 \\ 0 & 0 & S_v \end{bmatrix}. \quad (1)$$

The assumption that one of the principal stresses is vertical simplifies orientation of the stress tensor because the three principal stresses must be orthogonal to one another, so only one horizontal direction needs to be specified (Zoback, 2007). All stress directions provided in this report are the angle of S_H in degrees measured clockwise from geographic north.

Anderson (1905) synthesized three basic scenarios to describe a fault's movement at different stress states (Figure 2). A fault will slip normally when $S_V > S_H > S_h$, and such a stress regime is considered 'normal.' Similarly, stress regimes that allow strike-slip fault movement ($S_H > S_V > S_h$) and reverse (or thrust) fault

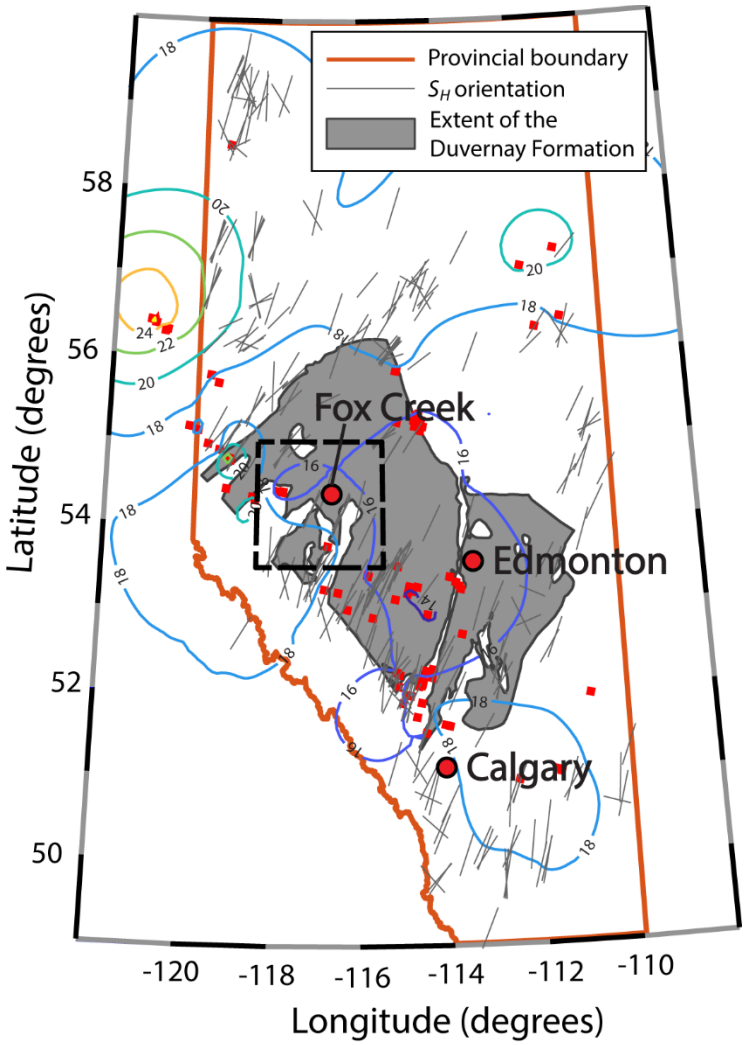

Figure 1. Location of the study area (thick dashed outline), extent of the Duvernay Formation described by Rokosh et al. (2012) in west-central Alberta, summary of information available in existing compilations of the directions of S_H from the World Stress Map (Reiter et al., 2014; Heidbach et al., 2016), and S_h gradients and locations of measurements (coloured contours and red dots; Haug and Bell, 2016) in Alberta and northeastern British Columbia.

movement ($S_H > S_h > S_V$) are categorized as strike-slip and reverse stress states. The determination of the vertical stress is often considered easier for the upper crust compared with its horizontal counterparts. The magnitude of S_V of a point in the relatively deep subsurface is equal to the total overburden pressure at that depth, which, in most of the Alberta Plains, can be calculated by integrating the density-dependent gravitational weight of the rocks overlying that depth. Evaluations of the magnitudes of in situ horizontal stresses are often subject to challenges and can only be reliably accomplished by drilling a borehole. Additionally, the uppermost crust is often saturated with fluid (i.e., groundwater, hydrocarbon). The fluid in the pore spaces within the rock will result in a non-zero pore pressure and will subsequently alter the effective stresses in the rock's matrix. Therefore, in studying stress states, it is also essential to have knowledge of the pore pressure (P_P), as this, via the concept of effective stress, influences the stress-dependent physical properties of rock in situ and is a significant factor in controlling rock failure and slip along pre-existing planes of weakness (see review in Schmitt et al., 2012). The reference hydrostatic pressure ($h(z)$) describes the variation in pore-fluid pressure with depth (z) expected in the crust when

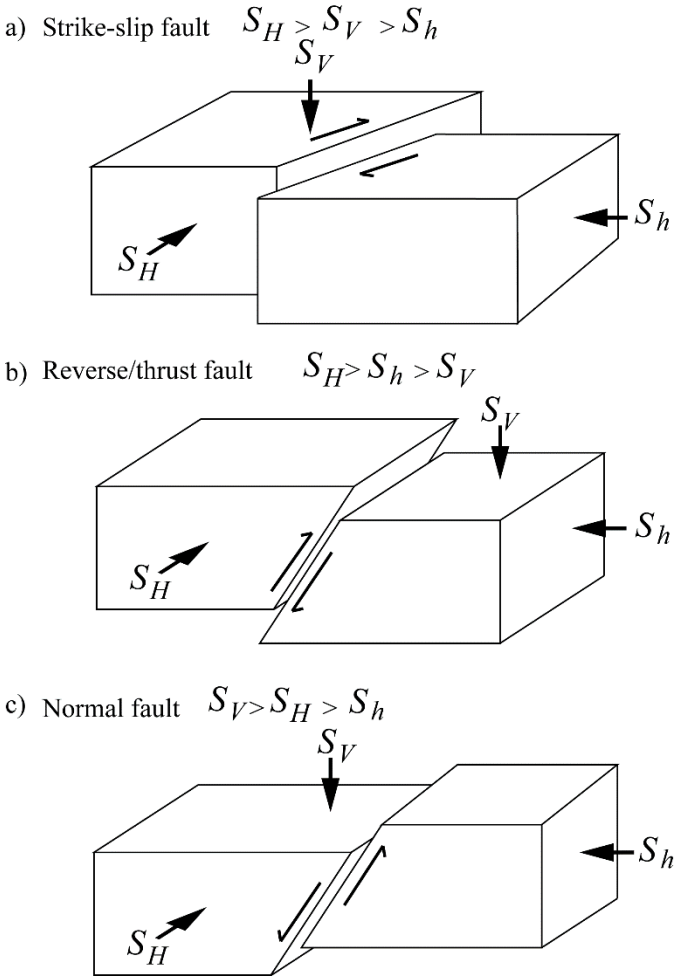

Figure 2. Anderson's faulting theory and stress regimes: a) strike-slip fault movement, when $S_H > S_V > S_h$; b) reverse or thrust fault movement, when $S_H > S_h > S_V$; and c) normal fault movement, when $S_V > S_H > S_h$.

rocks are fully water saturated from the surface downwards. The depth-dependent pressure head is given by

$$h(z) = -g\rho_w z\,, \tag{2}$$

where g is the acceleration due to gravity (assumed to be 9.8 m/s^2 in this case), ρ_w is the density of water (most commonly considered to be 1000 kg/m^3, with temperature and pressure effects ignored), and z is the depth below the surface. The reservoir is said to be overpressured or underpressured if the pore pressure at the specified depth exceeds or is less than $h(z)$, respectively.

All stress and pressure magnitudes are expressed using the SI unit 'pascal' (Pa, N/m^2), with kPa and MPa equating to 10^3 Pa and 10^6 Pa, respectively. Further, in line with standard practice in the geosciences, we assume the convention with compressive stresses and pressures having a positive sign and tensile stresses having a negative sign. Note that quantitative stress magnitudes and pore pressures are often reported in practice as gradients with their corresponding depth z. Some care must be taken with the 'gradients' as provided because they are almost always calculated from the ratio of a single measured value to the depth at which the measurement was made and, as such, can be misleading for practitioners when used to estimate values at other locations or depths. For example, the S_h gradient merely is $|S_h|/z$, which presumes

that $|S_h| = 0$ at the surface ($z = 0$). If this assumption is incorrect, then the extension of these results to different locations will result in incorrect estimation of the values. This approach can be more problematic should certain formations concentrate stresses based on the rock's mechanical properties (e.g., Plumb et al., 1991). In such a case, use of the gradient alone could lead to significant error when applied to formations whose depths differ from that where the measurement is made initially. To avoid this problem, we report directly all values of observed stress magnitudes and the depths from which the values originate in the accompanying digital datasets. That being said, maps of 'gradient' (the equivalent of the stress-to-depth ratio) of S_h, S_V and P_p are provided in Section 4 of this paper, in keeping with common industry practice.

2.2 Prior Stress Information in Alberta

The earliest developments in the analysis of borehole breakouts as indicators of in situ stresses came from the pioneering studies of geophysicist D.I. Gough at the University of Alberta and geologist J.S. Bell at the Geological Survey of Canada (Bell and Gough, 1979; Gough and Bell, 1981, 1982; Fordjor et al., 1983; Bell and Babcock, 1986; Woodland and Bell, 1989). They used the orientations from four-arm dip-meter logs from boreholes, some of which lie within the study area. These early studies stimulated a great deal of research, much of which is compiled within the current World Stress Map (Heidbach et al., 2016), although only stress directions are usually available. Morin (2017) provided a recent review of the stress determination literature in Alberta that begins with these early studies.

Bell et al. (1994) published the first comprehensive accumulation of the state of stress in the WCSB. In addition to stress directions obtained, at that time primarily from oriented dip-meter logs, they added analyses of a number of minifracture tests obtained across the WCSB to constrain the magnitude of the S_h. Bell and coauthors updated this work periodically (Bell and Bachu, 2003; Bell and Grasby, 2012), with the final compilation available for his data (Haug and Bell, 2016) including a total of 106 S_h measurements for northwestern B.C. and Alberta (Figure 1). The average S_h 'gradient' (S_h to depth ratio) for the Alberta Basin is estimated to be 19 kPa/m from the Haug and Bell (2016) dataset. The vertical stress S_V 'gradient' (S_V to depth ratio), on the other hand, is often considered to range roughly between 20 and 25 kPa/m in sedimentary rocks. The stress regime in Alberta is therefore assumed to be either strike-slip or normal.

On top of the dataset compiled by Bell and others, researchers have also attempted to provide additional data aimed at better constraining the regional stress orientations. The most recent version of the World Stress Map (WSM) provides a snapshot for the orientation of the stress tensor for most of the North American continent (Figure 1; Reiter et al., 2014; Heidbach et al., 2016), with most of the measurements recorded for the Alberta Basin obtained from older, oriented dip-meter logs (Babcock, 1978) arising from oil/gas exploration activities. A brief snapshot of the S_h 'gradient' is provided in a recent study by Fox and Soltanzadeh (2015), although the details of that analysis and the actual stress magnitudes were not made available for public access.

The orientation of S_H near Fox Creek is observed to be ~30–50°. Recent analysis of earthquakes recorded near Fox Creek shows dominant patterns of strike-slip faulting mechanisms, in agreement with previous S_h and S_V observations (Wang et al., 2016, 2017; Schultz et al., 2017). These focal mechanisms, together with aftershocks, suggest that the fault planes strike nearly north-south (i.e., 0° or 180°), indicating that the conjugate S_H orientation should be either 330° or 030°, assuming a frictional coefficient of 0.6. Similar angles of plate motion were also reported by Zoback and Zoback (1991) and Henton et al. (2006). Combining the findings from the previous studies, the in situ stress near Fox Creek is in the strike-slip stress regime, with S_H orientation of roughly 30°–50°.

The existing compilations in the WSM (Reiter et al., 2014) and the Haug and Bell (2016) report are useful and important. However, these datasets still lack the full set of components necessary for more informed interpretation of the stress state within the sector of the Kaybob assessment area near Fox Creek. In this report, we attempt to provide quantitative measures of the magnitudes of P_P, S_V, and S_h, and the

horizontal-stress directions. A preliminary constraint on the magnitude of S_H is also briefly discussed here.

3 Methodology

3.1 Determination of Vertical Stress (S_V)

As noted earlier, it is widely accepted that the vertical stress (S_V) at depths sufficiently below the influence of variations in the surface topography is nearly the overburden pressure and can be estimated by integration using the overlying rock densities $\rho(z)$ down from the surface to depth z as

$$S_V = g \int_0^z \rho(z) dz \, . \tag{3}$$

Geophysical density logs are commonly obtained for oil/gas exploration and development wells. The method relies on the attenuation of gamma rays originating from radioactive cesium; more information on density logging is available in Ellis and Singer (2007). The mass density is used primarily to provide an estimate of the rock porosity and secondarily as a lithology indicator. Here we use the logged density measurements directly to estimate vertical stress.

Despite the simplicity of Equation 3, two issues arise that complicate the use of such logs to estimate vertical stress:

1) Because the instrument used to determine density must be in contact with the borehole wall rock, the quality of such logs can vary depending on borehole conditions. The density of the sedimentary rocks in the study area could range broadly from about 2000 kg/m^3 for a highly porous, water-saturated Cretaceous sandstone to 2700 kg/m^3 for a nonporous Paleozoic limestone. For example, the poor-quality, raw density log shown by the blue lines in Figure 3a indicates a range of densities from <1500 kg^3 to >3000 kg/m^3; such extreme values are not reasonable and are likely due to rough borehole geometry that interferes with proper log operation. We overcame this limitation using a two-step process in which unreasonable outliers were first removed and then a 50 m wide, running-average smoothing filter was applied (orange line in Figure 3a). We estimated S_V magnitudes of ~90 MPa at 3500 m. This process was applied to density logs retrieved from more than 600 boreholes within the study area.
2) Density logs are often obtained only for depth intervals near the target formation, and only rarely are complete density logs available from the surface to the depth of interest. Significant gaps in the measured $\rho(z)$ along sections are often present in individual wells—particularly in the shallower depths (<500 m). This problem was partially overcome by using the available density logs, scattered both laterally and in depth, to create a final function that constructs a simple one-dimensional $\rho(z)$ using a statistical approach. For the sake of simplicity, we assumed that ρ is a function of z only. Hence, at any given depth, the associated value of ρ is obtained from kriging of all smoothed log ρ available from the same depth.

3.2 Determination of Minimal Horizontal Stress (S_h)

Operators will often invest in a pressure-transient well test that involves the creation of a small hydraulic fracture to constrain various geomechanical and reservoir parameters. Ideally, the pressure history of the section of an open borehole within which the fracture is created is isolated using pressurized packers to provide information that is useful in the design of the more robust hydraulic-fracture stimulation program. Briefly, the interval between the packers is pressurized until a fracture is created at the borehole wall. Pumping to the interval continues to extend the fracture into the formation. After pumping ceases, the interval is 'shut in' and the pressure $P_w(t)$ is allowed to decline naturally as the fluid in the borehole interval and the fracture permeates naturally into the formation. In principle, this decline curve may be interpreted to provide a host of geometric and flow-related parameters (Nolte, 1979; Schmitt and

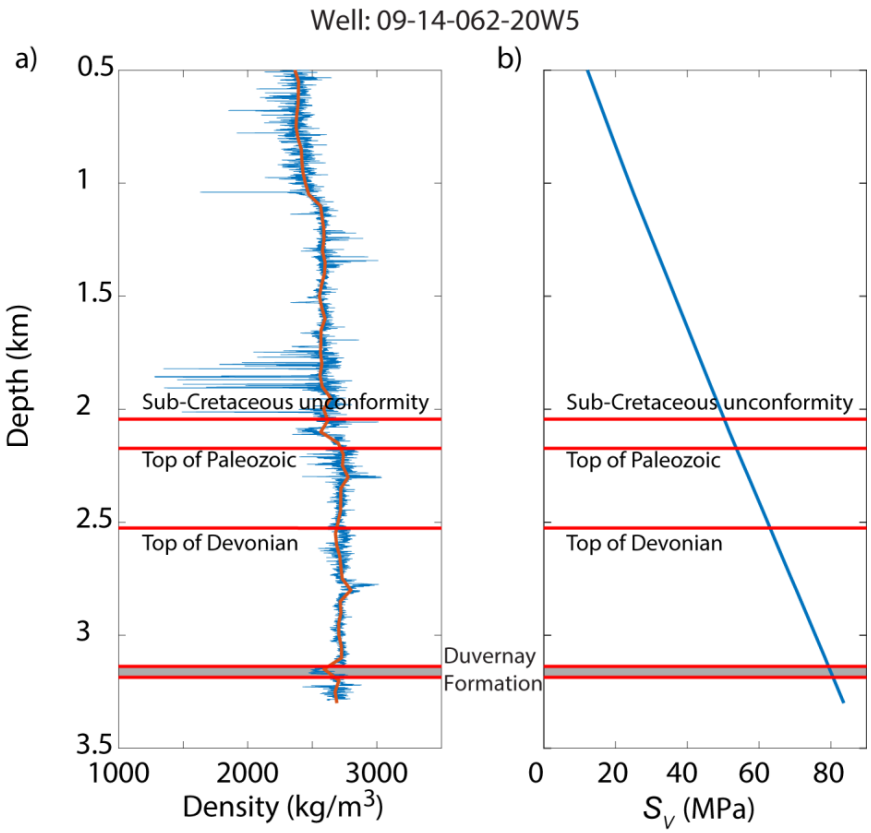

Figure 3. a) Example of a density log retrieved during this study; blue curve represents the original log, and the orange one represents the smoothed results for S_V modelling. b) Computed S_V from the density log shown in part a; density at depth <500 m is assumed to be equal to the smallest value from the smoothed density recordings (orange line in part a). Red lines show the boundaries of some geological units penetrated by the well.

Haimson, 2017). Here, we focus solely on the interpretation of such tests to obtain measures of the fracture-closure pressure (P_{FC}) and the formation-pore pressure (P_P).

The tests go by many names, such as microfrac, minifrac, and diagnostic fracture-injection test (DFIT). Currently in industry, the term DFIT is used widely but loosely, being applied to a wide variety of different wellbore-pressure tests significantly outside the scope of the proper multicycle pressure test. It is therefore important to know exactly how such tests were carried out. In this study, we include a number of DFITs carried out within a limited depth interval along the borehole that is isolated either by inflatable packers in an open hole or by perforations in a cased hole. Interpretation of the latter can be affected by restricted-flow effects through the perforations and by a potentially larger volume of fluid within the borehole, both of which lead to decreased ability to detect small changes in $P_w(t)$.

Figure 4 illustrates different time segments of an ideal $P_w(t)$ record, and fluid volume flowing into and out of the isolated interval. This process, and the interpretation of the decline curve $P_w(t)$, were described in detail by Schmitt and Haimson (2017), so only a brief overview is given here. Figure 4 is meant only to illustrate various time segments during the DFIT testing and is not drawn to proper scale with respect to pressure or time. These segments are as follows:

- The initial pressure P_{EQ} within the sealed interval is assumed to be at equilibrium before the test. Pressurization of the interval commences with pressure increasing until a tensile fracture from the interval into the rock mass initiates at P_{FI}, followed by unstable-fracture propagation into the formation at the breakdown pressure (P_b), which we here take to be the reference time t_0.

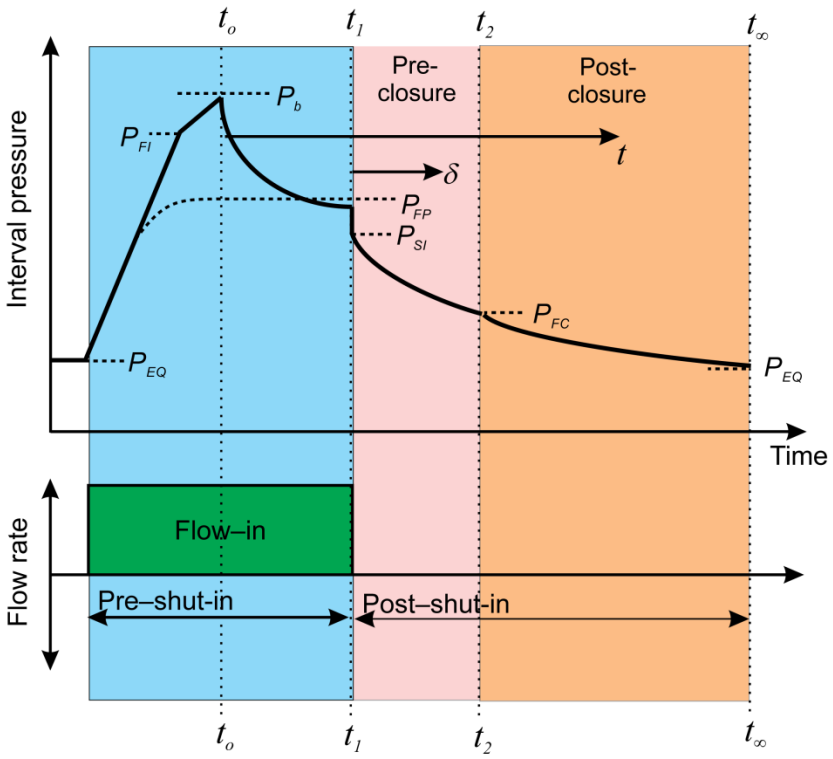

Figure 4. Different phases of fluid flow during the diagnostic fluid-injection test: pre–shut-in (blue), pre-closure (pink), and post-closure (brown).

- Pumping of fluids to the interval may continue to extend further the induced fracture. This fracture-propagation pressure (P_{FP}) may be controlled by numerous factors, such as fluid viscosity and whether the measurement is carried out in an open borehole or through perforations in a cased borehole. Pumping stops and the interval and open fracture are shut in at t_1, with the pressure dropping rapidly to the shut-in pressure P_{SI} (see blue section in Figure 4).
- In the post–shut-in period immediately following time t_1, it is assumed that the induced fracture remains propped open by the interval pressure $P_w(t)$. However, $P_w(t)$ declines during this shut-in period due to 'leak-off' flow to the formation from the still-open induced fracture and, in open-hole situations, the sealed borehole interval (see pink section in Figure 4).
- At time t_2, the fracture-closure pressure (P_{FC}) is reached. It is usually assumed that P_{FC} is the lowest pressure required to keep the hydraulic fracture open; as such, it is equal to the magnitude for minimum principal stress σ_3, although Detournay et al. (1989) suggested, based on consideration of poroelastic effects, that $P_{FC} > \sigma_3$. Consequently, accurate determination of P_{FC} is a key goal in the DFIT $P_w(t)$ analyses (see brown section in Figure 4).

The post-closure leak-off continues after t_2, with $P_w(t)$ continuing to decline until it eventually, given sufficient time, equilibrates with the pore pressure P_{EQ} within the formation. Furthermore, the pressure-drawdown curve can be extrapolated to estimate the wellbore pressure at the infinite shut-in time. The extrapolated reservoir pressures from DFITs, on the other hand, provide constraints on the pore pressure of the rocks near the wellbore.

Different plotting strategies, in which the dependent and independent axes are various functions, transformations, or derivatives of $P_w(t)$ versus t, respectively, have been developed to identify the point at which the fluid pressure P_{FC} is barely large enough to keep the fractures open. Some of these strategies are reviewed in Schmitt and Haimson (2017) and Craig et al. (2017). Barree et al. (2009) and Craig et al. (2017) further re-examined available field and laboratory $P_w(t)$ determinations and suggested that a

'holistic' combination of *G-function* derivative, square-root time, and log-log plotting be employed, which they illustrated with some examples. Recently, questions have also been raised regarding the validity of the *G function* and its underlying assumptions in the low–leak-off shale formations such as the Duvernay (Zanganeh et al., 2018). Obtaining consistent measures for P_{FC} from these various visualization-enhancement methods lends credence to a proper interpretation. Fluid flow through the wellbore into the hydraulically induced fractures can be divided into pre-closure and post-closure phases, as previously discussed. There is still debate regarding how flow regime would change in response to fracture closure and the corresponding impacts on the recorded pressure history in the wellbore. Most researchers have come to agree that one could, in principle, identify fracture closure through the slope change in the pressure history. Plotting pressure history in either *log(t)* versus *log* (p_w) or *log (t)* versus p_w, which amplifies such slope change, has been successfully applied to the interpretation of downhole flow phases (Doe et al., 1981; Haimson and Rummel, 1982).

Cinco-Ley (1981) further proposed that the fluid flow near the wellbore can be categorized into four regimes (Figure 5). Assuming that fluid leak-off in the fractures is minimal in tight and impermeable formation rocks, Cinco-Ley's flow regimes can be essentially reduced to only linear (Figure 5a) and radial

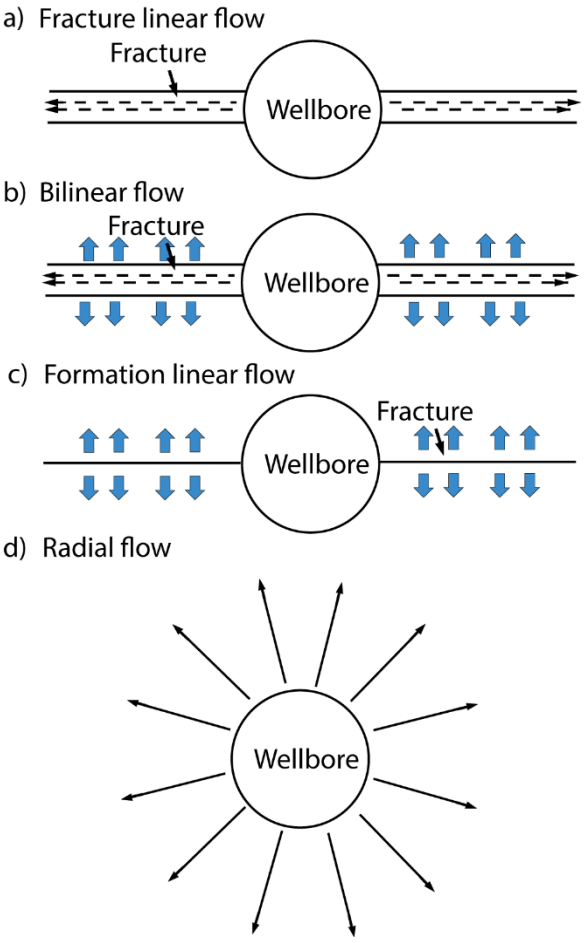

Figure 5. Four near-wellbore fluid-flow regimes proposed by Cinco-Ley (1981): a) fracture linear flow, with fluid flowing in the direction of fractures; b) bilinear flow, with fluid flowing in the direction of fractures and also leaking into the nearby formation; c) formation linear flow, with fluid flowing from the fractures to the nearby formation rocks in a direction perpendicular to that of the fractures; and d) radial flow, with fluid flowing outwards radially from the wellbore to the nearby formations.

flows (Figure 5d), and the pressure drop and time follows the relationship $log\ t \propto log\ \Delta p$ (Barree et al., 2009). It is possible to delineate P_{FC} using plots of $log[P_w(t)]$ versus $log(t)$ or $P_w(t)$ *versus* $log(t)$. One could, in principle, obtain a measure of P_{FC} by finding where the $log[P_w(t)]$ versus $log[t]$ plot deviates from this slope (or one near it). In practice, this is not so easily accomplished (e.g., Barree et al., 2009, Figure 3), so we used the linear portion of this curve near the inflection point (see below for example) to initially limit the range of possible values for P_{FC}.

The downhole fluid flow becomes much more complicated for more permeable formation rocks when fracture growth and pressure-dependent fluid leak-offs happen with comparable magnitudes. Following the assumptions laid out by R.D. Carter (see Howard and Fast, 1957, Appendix I), namely that 1) the fractures have a uniform width, and 2) the flow in the fracture is linear in the direction perpendicular to the fracture face, the Carter leak-off is widely assumed by industry practitioners to describe the flow rate as being inversely proportional to $\sqrt{t}$ where t is the total injection time. In Howard and Fast (1957), it is further assumed that fluid velocity is uniform across the fracture, so the 'Carter' leak-off equation can be presented as

$$q(t) = C_L/\sqrt{t}\,, \tag{4}$$

where q is the fluid-loss rate and C_L is the fracturing-fluid coefficient that describes the resistance for the fluid leaking off to the formations. C_L is commonly referred as 'Carter's leak-off coefficient' by industry. The analyses below incorporate this underlying assumption.

The first transformation of the pressure draw-down (Figure 6a), resulting from fluid leak-off from the borehole, is predicated on the assumption of a linear flow regime, following Cinco-Ley (1981), in which $P_w(t)$ changes proportionally to $\sqrt{t}$. Consequently, the locus of $P_w(t)$ versus $\sqrt{t}$ would be a straight line (Figure 6b), the point of deviation from which would indicate P_{FC}. Barree et al. (2009) noted that use of this criterion in practice leads to an early pick of fracture closure (overestimated P_{FC}) and suggested the use of the inflection point that may more readily be found from the derivative $dP_w(t)/d\sqrt{t}$ plot. This behaviour is further enhanced in the semilog derivative $\sqrt{t}\ dP_w(t)/d\sqrt{t}$ curve, with P_{FC} declared at the point of departure of its trajectory from the initial linear increase.

Nolte (1979) further extended Carter's assumption with a fixed vertical height of fracture and described a linear relationship between pressure and a dimensionless shut-in time using the proposed *G function*. In Nolte's formulation, Carter leak-off is modified to account for the horizontal growth of the fracture. Nolte assumed the fracture would grow linearly with time during the pumping stage, so the Carter leak-off coefficient would be proportionally dependent on the pumping time. Pressure-dependent leak-off is also considered in Nolte's formulation.

Consequently, the second important standard procedure (Figure 6c) employed to estimate P_{FC} relies on what is referred to as *G-function* analysis. The relationship between time and wellbore pressure is given in terms of a dimensionless shut-in time $\delta = [t - t_1]/t_1$ for $t > t_1$ (Nolte, 1979). Time (t) accumulates only after the fracture is created at a time t_0, presumed to be the initiation of fracture propagation (Barree et al., 2009). The use of such forms of dimensionless times follows from earlier work by Horner (1951):

$$\Delta P(\delta_o, \delta) = P^* G(\delta_o, \delta)\,, \tag{5}$$

where P^* is the 'Nolte match pressure' (Castillo, 1987), which is a constant depending on a variety of parameters that control the loss of fluids from the fracture, fracture geometry, the fracture's 'age' (i.e., $t_1 - t_o$), and normalized pressures within the fracture (Nolte, 1979; Castillo, 1987). We mostly ignored the effect of these in this study, as the determination of P_{FC} depends more on the details of the behaviour of the pressure-decline curve, but we note that analysis of the decline curves can conversely provide some of this information. Indeed, Nolte's (1979, 1986) original intent was to deduce the fracture geometry, and flow constraints from the post–shut-in pressure-decline curve, using knowledge of P_{FC} obtained using

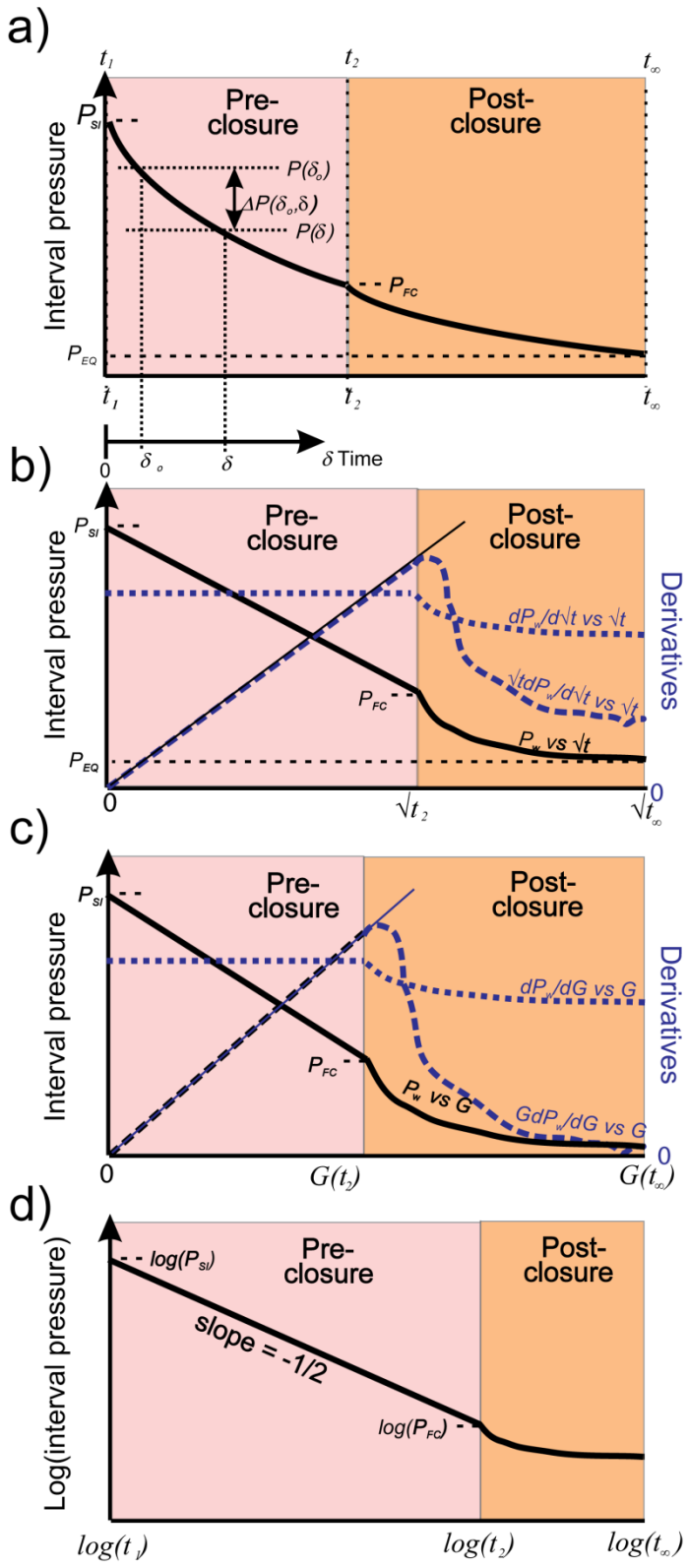

Figure 6. Transformations of the diagnostic fluid-injection test (DFIT) pressure history for use in constraining fracture-closure pressure (P_{FC}): a) fall-off curve of the wellbore pressure following the shut-in; b) $\sqrt{t}$ plot assuming Carter leak-off; c) *G-function* plot initially proposed by Nolte (1979); and d) *log(t)* versus *log(P_w)* plot.

other methods (Nolte, 1979, Figure 8). More germane to the current discussion, the time-dependent *G function* is

$$G(\delta_o,\delta)=\frac{4}{\pi}[g(\delta)-g(\delta_o)] \quad . \tag{6}$$

The function for the limiting case with small leak-off into the growing fracture during its growth in the pressurization period is

$$g(\delta)=\frac{4}{3}\left[(1+\delta)^{3/2}-\delta^{3/2}-1\right] \tag{7}$$

or

$$g(\delta)=(1+\delta)\arcsin\left[\frac{1}{(1+\delta)^{1/2}}\right]+\delta^{1/2} \quad . \tag{8}$$

For the case where there is substantial leak-off in more permeable formations, Barree et al. (2009) used $\delta_o = 0$ at $t = t_1$. Both of the intermediate functions (high leak-off and low leak-off) in reality give similar results, and here we use the low leak-off form (Equation 7), given the expected low permeability within the Duvernay Formation.

Castillo (1987) exploited the linearity of Equation 5, noting that a plot of $P_w(t))$ versus $G(\delta_o,\delta)$ is a line during the post-closure fluid leak-off period in Figure 6b, with a slope equal to P^* and an intercept of P_{SI}. Consequently, he suggested that this plot would deviate from a line at P_{FC}. Detection of this point is further enhanced in the plot of $dP_w(t)/dG$ versus $G(\delta_o,\delta)$, which would remain at the constant value of P^* during the decline period and change slope after closure. As with the $\sqrt{t}$ plotting, the initial section of the plot of the semilog derivative $GdP_w(t)/dG$ should be a line passing through the origin, with P_{FC} declared at the point where $GdP_w(t)/dG$ leaves this line (Barree et al., 2009).

Finally, curves related to log[$P_w(t)$] versus log[t] may also be employed to delineate P_{FC}. For the ideal case, pressure decline for a fracture linear flow in the post–shut-in period, the slope of this curve is expected to be –½ (Figure 6d). Again, one could in principle obtain a measure of P_{FC} by finding where the log[$P_w(t)$] versus log[t] plot deviates from this slope (or one near it). In practice, this is not so easily accomplished (e.g., Barree et al., 2009, Figure 3) and here we employ the linear portion of this curve to initially limit the range of possible values for P_{FC}.

The procedure used to constrain P_{FC} in this study is illustrated in Figure 7, which begins with a plot of $P_w(t)$ versus t (Figure 7a) for 180 hours for the test in well 01-11-034-24W4 at 2157.5 m depth. The operational procedures of this test were not detailed in the report submitted to the Alberta Energy Regulator by the operators. Because of this, assumptions were made that the injection begins when the wellbore fluid pressure starts rising, as recorded by the pressure gauge at 0 h. The well is considered shut-in when a sudden pressure drop is observed at ~0.09 h (see Figure 7a).

The curves in the *log[$P_w(t)$]* versus *log[t]* plot (Figure 7b) and the [$P_w(t)$] versus *log[t]* plot (Figure 7c) display a linear section that we interpret to correspond to the fracture linear flow (see Figure 5a). This linear fit of the log-scale curve corresponds to a P_{FC} between 21.9 and 23.0 MPa (see Figure 7b and c) at ~4 hours after shut-in. With the constraint range of P_{FC} obtained through the *log(t)*-based plots, the *G-function* and $\sqrt{t}$ plots (Figure 7d and e) are investigated to further refine the timing of fracture closure. In this example, the estimated P_{FC} through *G-function* analysis is 22.9 MPa, which falls within the range constraint of P_{FC} obtained through the log(t)-based plots. The $\sqrt{t}$ plot shows a P_{FC} of 22.9 MPa , roughly the same (these numbers are rounded) as was estimated through the *G function* analysis (22.9 MPa),

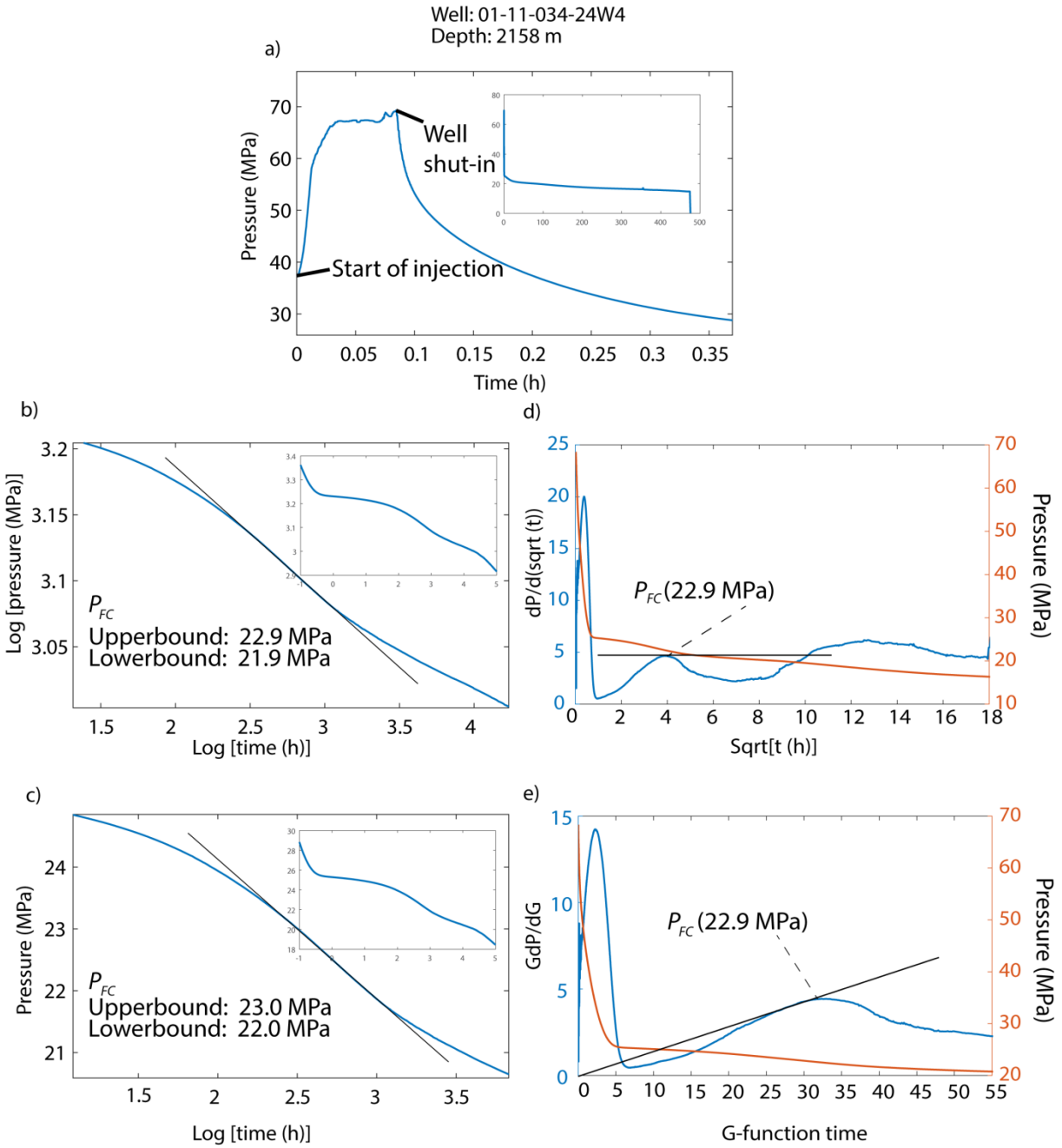

Figure 7. Diagnostic fluid-injection test (DFIT) data and analysis from well 01-11-034-24W4, with pressures recorded by a pressure gauge at surface: a) recorded pressure history from the DFIT, showing the moment when the well is shut in after the hydraulic fractures are created; inset shows the entire injection/shut-in history; the shut-in period is many times longer than the injection period to allow wellbore pressure to reduce to fracture-closure pressure and close to pore pressure of the surrounding formation rocks; b) log*(P_w) versus* log*(t)* plot constraining P_{FC} at ~22.9 MPa; c) *P_w versus log(t)* plot constraining P_{FC} at 22.0–23.1 MPa; d) √t plots estimate the P_{FC} at 22.9 MPa, the left axis showing the values of dp/d(√t) and the right axis showing the corresponding pressures at the same time; e) *G-function* plots estimate P_{FC} at 22.9 MPa, the left axis showing the values of GdP/dG and the right axis showing the corresponding pressures at the same time.

indicating a minimal amount of fluid leak-off, as expected for this low-permeability formation. The consistency in the constraining P_{FC} using various methods provides credence for our approach. The success of this approach can be at least partially attributed to the fact that the low permeability of the Duvernay Formation limits the amount of pressure-dependent leak-off, which could present challenges for more permeable formations.

In some cases, the pressure history is recorded with a pressure gauge at the surface, so the actual downhole pressure can be estimated as $P_w = P + P_h$, where P_h is the hydrostatic pressure at the depth of measurement. When a detailed description of fluid properties was not provided in an operator's report, we assumed that the wellbore fluid had a specific weight of 9.8 kN/m^3. Therefore, the minimum horizontal stress is constrained between 43.0 and 44.2 MPa. One could also, in principle, estimate the breakdown pressure from the maximum value of the recorded pressure history and then estimate the maximum horizontal stress. However, without detailed knowledge of the operations of this test and the mechanical properties of the formation rocks, such an estimate would only be speculative.

Ideally, the DFIT should be conducted in 'open-hole' conditions immediately after the borehole is drilled. Nevertheless, operators may conduct the DFITs through perforated casing that has already been installed for engineering-practicality reasons. In principle, the interpretations of the 'cased-hole' DFITs follow the same procedures as the 'open-hole' test. The cased-hole test results may be more uncertain due to complications caused by restrictions in fluid flow through the casing and cement. According to the submitted industry reports, all of the DFITs that provided data for this study were carried out in 'open-hole' conditions.

3.3 Determination of Formation Pore Pressure (*Pp*)

Formation pore pressure can be constrained by a number of well-testing techniques, including static-gradient tests, flow/buildup tests, and post-closure DFIT analysis. The fluid flow from or into the wellbore is driven by the pressure difference between the wellbore and the fluid/pore pressures in the surrounding rocks. The formation-fluid pressure can be indirectly determined by measuring the wellbore pressure and fluid-flow rate. That being said, there are arguments for and against the use of these well-testing techniques in different circumstances. In this section, we briefly discuss the measurement of pore pressure using each of these methods.

Static-gradient surveys assume that the flow from the reservoir to the borehole has reached a steady state after a sufficiently long time (t_∞), such that an equilibrium $P_w(t) \rightarrow P_{EQ} = P_P$ has been attained. Such an assumption may be valid if the flow rate is meager, with only a small amount of fluid extracted from the reservoir, and reservoir pressure near the wellbore is not affected by the fluid extraction. A static-gradient survey is often performed by placing a pressure gauge downhole to obtain the fluid pressure at a certain depth. This type of survey is regularly conducted in cased holes, so linear extrapolation with assumed or calculated fluid density is needed to estimate the fluid pressure at the depth of the perforations, where the borehole fluid pressure is considered equivalent to that of the surrounding geological formation. The pressure calculated for the mid-point of perforations (MPP) is typically considered a loose constraint for the fluid pressure in the nearby geological formations. The static-gradient test will often be performed at multiple points along a cased wellbore, primarily because it can be done easily, to obtain the averaged MPP pressure through linear extrapolation.

The static-gradient survey is often followed by a transient pressure test to obtain a more reliable constraint on formation-fluid pressure. Flow and build-up tests often start with lowering the pressure $P_w(t)$ by extracting fluid from the wellbore for a period of time. The wellbore is then shut in to allow reservoir fluids to flow back in with a corresponding increase in $P_w(t)$ that depends on the pressure differentials and the reservoir fluid mobility. In principle for a reservoir of infinite extent, the wellbore fluid pressure $P_w(t)$ will in infinite time approach the limiting reservoir pressure P_P. In practice, the time allowed for such tests is restricted by practical considerations and, to overcome this problem, workers instead have developed methods to extrapolate an observed $P_w(t)$ to estimate the P_P.

Analytical solutions for the pressure-time functions of different flow regimes can be derived and compared with the wellbore-pressure history to extrapolate the reservoir pressures. The pressure-time functions of borehole fluid flow for different flow regimes are usually presented in the following form:

$$P - P_w = C * F(t)\,, \tag{9}$$

where *t* is the 'equivalent flow time', which is a function of the flow time of the testing well, and *F* is an arbitrary function of time. For a buildup test, the equivalent flow time should approach a constant limit when the actual shut-in time is infinitely large, in order for P_w to approach *P*. Plotting the wellbore pressure against the equivalent time allows extrapolations of the pressure history approaching such a limit and therefore provides an estimation of wellbore pressures at an infinitely long shut-in time. Estimation of fluid pressure using linear and radial fracture-flow assumptions, which are the two most extreme scenarios, will provide range constraints for the actual formation-fluid pressure.

For an unfractured wellbore, radial fluid flow dominates (Figure 5d) and, assuming a flow rate of *q*, the wellbore's fluid pressure will take the following form:

$$P_w = P - qBlog(t)\,, \tag{10}$$

where *q* is the flow rate and *B* is a constant that depends on wellbore geometry, fluid properties, and formation permeability. Horner (1951) proposed an approach to predict the wellbore pressure after borehole shut-in using the superposition of fluid flow. It is assumed that, after the shut-in, a fluid injection with a rate equal to that of the flow-out rate before shut-in is introduced while the fluid is still flowing out of the wellbore at the same rate. The total fluid-flow rate in the wellbore remains equal to zero, and the pressure changes in the borehole will be equal to the superposed pressure change from the fluid flow out and the fluid injection (Figure 8a). An approximate solution for the fluid-pressure change in the wellbore can therefore be established as

$$P_w = P - qBlog(\Delta t) + qBlog\left(t_p + \Delta t\right), \tag{11}$$

where Δt is the shut-in time or the injection time for the hypothetical injection flow and t_p is the flow-out time before the injection. The so-called 'Horner time' (Horner, 1951) can therefore be defined as

$$F_H = log\left(\frac{t_p+\Delta t}{\Delta t}\right), \tag{12}$$

where t_p is the production time before well shut-in and Δt is the time elapsed after shut-in.

Following the Horner equation (Horner, 1951) and assuming a radial wellbore flow, the wellbore pressure at the infinitely long shut-in time can be obtained by identifying the linear trend in the Horner plot at the end of the buildup stage and extrapolating it to intercept with the t = 1 point, where $\Delta t = \infty$. If the formation surrounding the wellbore is fractured, linear fracture flow needs to be considered instead of radial flow, so the linear flow equation (Equation 11; Ahmed and McKinney, 2011) would be applied to extrapolate the final wellbore shut-in pressure using the similar superposition principal

$$P_w = P_{initial} - qB\left[\sqrt{\Delta t} - \sqrt{t_c + \Delta t}\right], \tag{13}$$

in which $qB\sqrt{\Delta t}$ accounts for the hypothetical injection flow and $qB\sqrt{t_c + \Delta t}$ represents the pressure change due to fluid flow out. Subsequently, the equivalent time for linear fracture flow can be expressed as

$$F_H = -\sqrt{\Delta t} + \sqrt{t_c + \Delta t}\,. \tag{14}$$

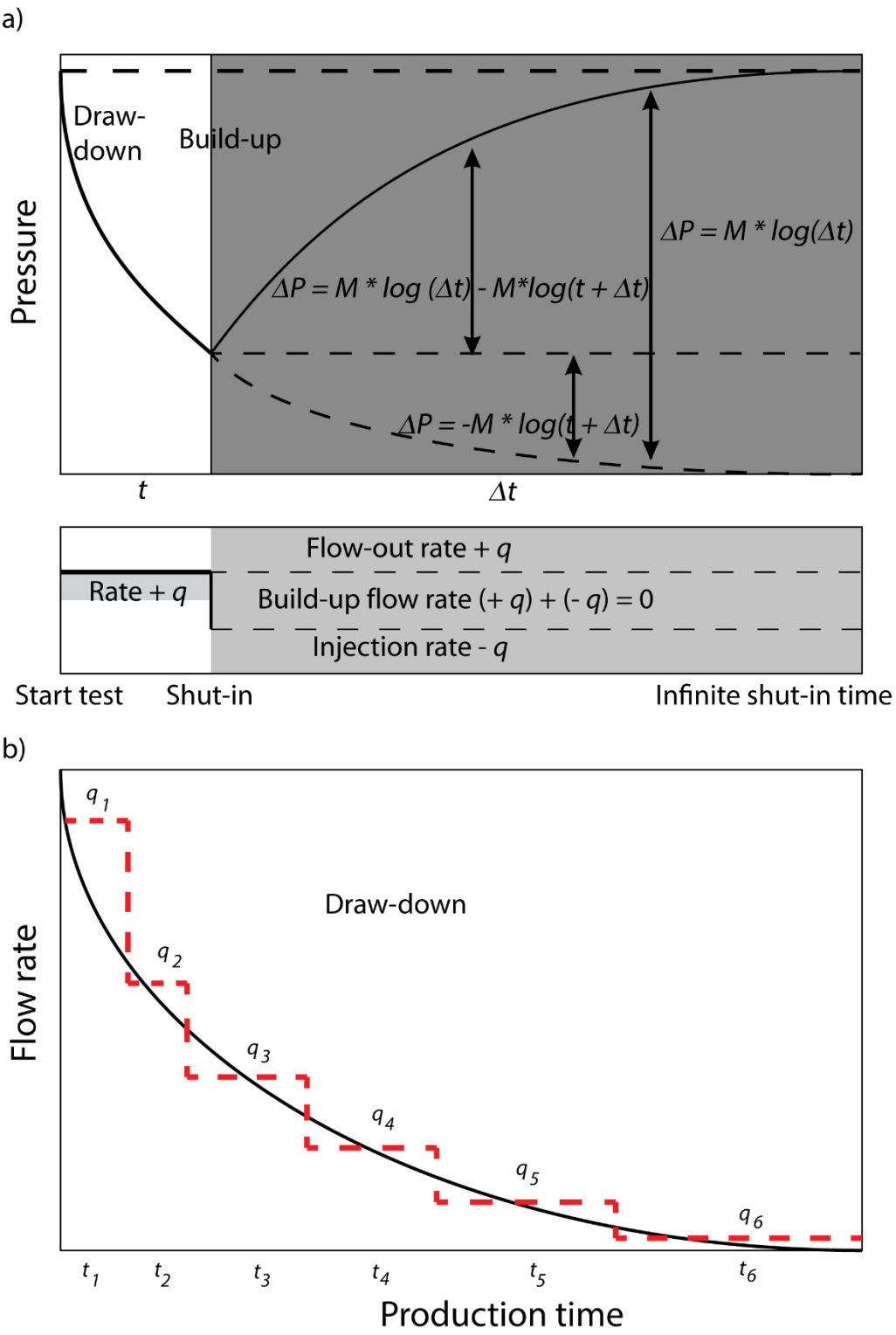

Figure 8. Conceptual illustration showing the superposed fluid flow in the borehole: a) schematic showing the flow and buildup phases of the test and the principle of superposition; following the shut-in of the well, it is assumed that the wellbore fluid will continue to flow out (dashed line) and an injection of fluid at the same rate will result in a net zero flow rate; b) step function for varying flow rate, the solid line representing the flow rate that can be numerically represented by a step function (red dashed line).

In this case, F_H is linearly proportional to the wellbore pressure (P_w). The linear fracture Horner time also approaches 0 at the infinitely long shut-in time. Following a similar approach, the initial formation pressure can be estimated by extrapolating the linear trends in the linear Horner time plot and finding its intercept with t = 0.

Equations 11 and 13 assume that the flow rate in a wellbore is constant. In case the flow rate is not constant, the flow history can be divided into a step function of many segments of time within which the flow rate is constant (Figure 8b). Equations 11 and 13 can therefore be rearranged to represent the superposition of the multiple steps with different flow rates as

$$t_h = \sum_{j=1}^{n} \frac{q_j - q_{j-1}}{q_n} \sqrt{t - t_{j-1}} \quad (15)$$

for linear flow and

$$t_h = \sum_{j=1}^{n} \frac{q_j - q_{j-1}}{q_n} log(t - t_{j-1}) \quad (16)$$

for radial flow. In Equations 15 and 16, q_j represents the flow rate at each step; t_j is the corresponding flow time; t_h is the superposed linear or radial time; and q_n is proposed to be the final flow rate in the wellbore before shut-in, although it does not mathematically impact the extrapolated eventual shut-in pressure. In this study, the superposed time plots are used when the flow rate is reported for the well testing. In cases when the flow rate is not available, a constant flow rate is assumed from when the well starts flowing until shut-in.

An example (well 08-32-046-09W5, TVD 3140 m) is provided here for identifying formation-fluid pressure using the superpositioned linear- and radial-flow assumptions. Figure 9a shows the pressure history recorded for the flow-buildup test, with the final wellbore pressure recorded at 47.5 MPa. The extrapolated $P_w(t)$ at the infinite shut-in time is estimated to be between 48.9 and 51.3 MPa.

Similar to the flow-buildup test, the pressure history of the DFIT after fracture closure provides an indication of the reservoir pressure. Notably, the extrapolations of Nolte (1979) and Soliman et al. (2005) are commonly used to determine the theoretical wellbore pressure (P_w) for the infinitely long shut-in time, which should be equal to the initial undisturbed formation-fluid pressure.

Soliman et al. (2005) proposed that, if the flow is radial, the wellbore pressure can be expressed as

$$P_w = P_i + M * \frac{1}{t_p + \Delta t} \quad (17)$$

and, for linear fracture flow, as

$$P_w = P_i + M * \sqrt{\frac{1}{t_p + \Delta t}}, \quad (18)$$

where t_p is the production/injection time and Δt represents the time elapsed after shut-in.

For both scenarios, the equivalent time is bounded between 1 (well shut-in time) and 0 (infinite time after shut-in). Linear extrapolations of the P_w linear/radial equivalent time to intercept with the time axis at 0 yields an estimation of initial reservoir/formation pressure.

Nolte (1979) also proposed the relationships

$$P_w = P_i + M * log(1 + \frac{16}{\pi^2} * t_c/(t - t_c)) \quad (19)$$

for radial flow and

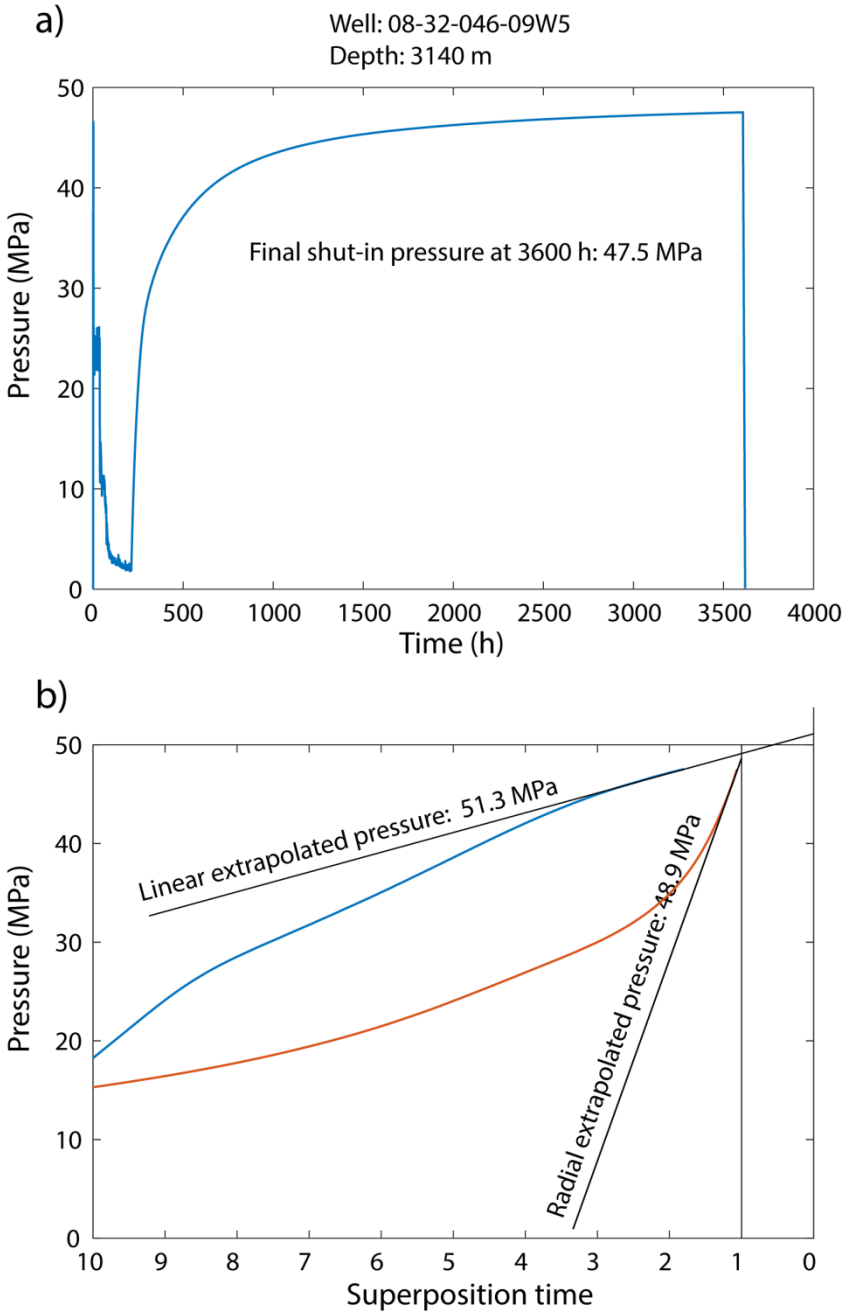

Figure 9. Sample analysis of a flow-buildup test: a) recorded pressure history during the test; and b) extrapolated pressures with the linear-flow and radial-flow assumptions using the superposition principle.

$$P_w = P_i + M * \left(\sqrt{1 + \pi^2 * \frac{t-t_c}{16t_c}} - \sqrt{\pi^2 * \frac{t-t_c}{16t_c}}\right) \quad (20)$$

for linear fracture flow. Where t_c stands for the fracture closure time and t is the cumulative test time.

A linear relationship between the proposed equivalent time F and wellbore pressure can be established, using Soliman-Craig or Nolte's approach, respectively, as

$$F_L = \frac{1}{t_p + \Delta t} \text{ or } F_L = \sqrt{1 + \pi^2 * \frac{t - t_c}{16 t_c}} - \sqrt{\pi^2 * \frac{t - t_c}{16 t_c}} \quad (21)$$

for linear fracture flow and

$$F_R = \sqrt{\frac{1}{t_p + \Delta t}} \text{ or } F_L = log(1 + \frac{16}{\pi^2} * t_c/(t - t_c)) \quad (22)$$

for radial flow. Extrapolation of the linear trends of F_L versus P_w or F_R versus P_w and finding their intercept with F = 0 (infinite shut-in time) allows reservoir fluid pressures of the undisturbed state to be constrained.

Figure 10 shows an example of a well-testing result (well 01-11-034-24W4) at a depth of 2158 m, with the eventual shut-in pressures estimated by Nolte and Soliman-Craig linear/radial plots. The eventual shut-in pressure recorded by surface pressure gauge for this test is constrained between 12.5 and 14.5 MPa using Nolte's approach and between 12.1 and 14.6 MPa using the Soliman-Craig solutions. As mentioned earlier, the pressure history for this test was recorded by surface pressure gauges, so the actual downhole pressures at the measurement depth need to be computed by adding the hydrostatic pressures. Assuming a water density of 1000 kg/m^3 and gravitational acceleration of 9.8 m/s^2, the results from this test constrained the formation pressure to between 33.2 and 34.7 MPa. The kinks near the ends of both pressure-history curves in Figure 10 can be caused by operators pulling off the pressure gauges at the end of testing, causing artifacts at the end of the curves.

In this study, we recorded the pore pressure extrapolated using the Soliman-Craig and Nolte methods for each of the DFITs collected. Horner linear and radial extrapolations were applied to the analysis for the flow and buildup tests, and both results estimated assuming linear fracture flow and radial flow. Note that the actual fluid flow in the wellbore is more complicated than the assumptions laid out above. To accurately determine the real reservoir pressure, adequate modelling and history matching are needed; however, due to the limitation of time and resources, we do not extend our discussion to the modelling of wellbore fluid flow. That being said, the actual pore pressure of the nearby formation rocks is constrained by the results estimated based on the assumption of flow regimes being linear or radial. In the accompanying datasets, pore-pressure estimates from the methods described above are recorded for each test analyzed in this study.

3.4 Determination of Directions and Magnitudes of S_H

Bell and Gough (1979) and Gough and Bell (1981) first noticed, from examination of oriented dip-meter logs, that the elongation of the cross-sections of deep vertical boreholes in western Alberta is consistently oriented northeast-southwest. They surmised that these features originated from the azimuthal variations of the horizontal-stress concentrations (S_H and S_h), causing shear compressive failure of the borehole wall centred on the borehole's spring line pointing in the S_h direction. This failure leads to spalling of the rock from the borehole wall elongating the borehole's radius in this direction; these elongations are now commonly referred to as borehole breakouts. Consequently, determining the horizontal-stress directions is done relatively simply by finding the azimuths of the borehole breakouts (BO) using oriented calipers or image logs.

Similarly, the hoop stresses on borehole spring-line azimuths aligned with S_H are most prone to pure tensile failure; this can result in drilling-induced tensile fractures (DITF) being created on the borehole wall. If these exist, their azimuth will likewise directly indicate the S_H direction.

Although controversial, the existence and dimensions of BOs and DITFs are often used to constrain stress magnitudes. To do this, one requires knowledge of the rock strengths, which are often difficult to obtain, particularly in the absence of core for direct measurements. Barton et al. (1988) provided a formula that combines the observed angular width Θ of a breakout with knowledge of the rock's unconfined

compressive strength (UCS) and an independently determined measure of the magnitude of S_h (usually from the fracture-closure pressure [P_{FC}] determined in the pressure-decline analyses described earlier) to constrain the magnitude of S_H:

$$S_H = \frac{UCS + P_P + P_w - S_h(1-2\cos T)}{1+2\cos T}. \quad (23)$$

We will employ this formula later to estimate S_H. Note, however, that to simplify the number of variables required, Equation 23 does not correctly incorporate a true Mohr-Coulomb failure criterion, thus biasing the results. In later contributions we provide updated expressions to account for more realistic rock behaviour.

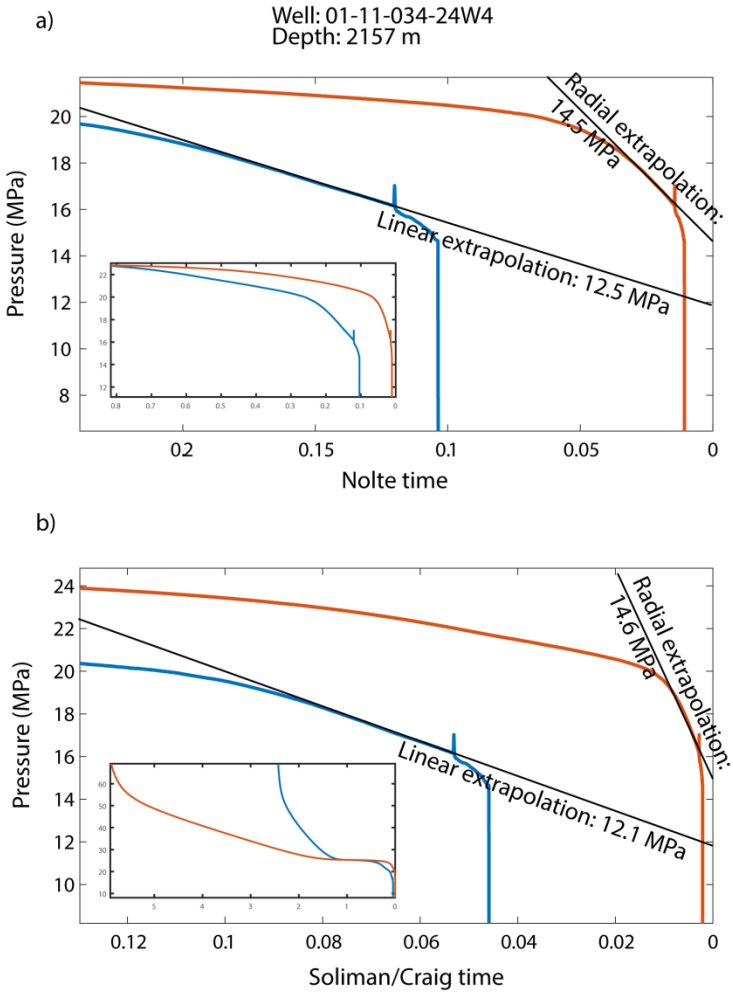

Figure 10. Sample post-closure analysis to extrapolate the formation pore pressure: a) using Nolte's approach with assumptions for both linear (blue line) and radial (orange line) flow regimes, respectively; black lines show the extrapolated final wellbore pressure following these two assumed flow regimes; b) using the Soliman-Craig approach (blue and orange lines for linear and radial flow, respectively) with the same assumptions as part a; large plot shows the last part of the measurement when the linear extrapolation is evaluated, with the entire analysis shown in the inset.

In this study, oriented wellbore-image logs are analyzed to constrain the orientation of horizontal stresses. The borehole images used for this study are logged using either an ultrasonic borehole televiewer or a microresistivity imaging device (e.g., Ultrasonic Borehole Imager [UBI™] or Fullbore Formation Microimager [FMI™]). Both tools have proven useful in determining the geometry of boreholes in order to identify BOs and DITFs. An example of a portion of an ultrasonic-image log containing both BOs and DITFs is given in Figure 11. Further details on the theory of the formation and interpretation of such features can be found in Schmitt et al. (2012).

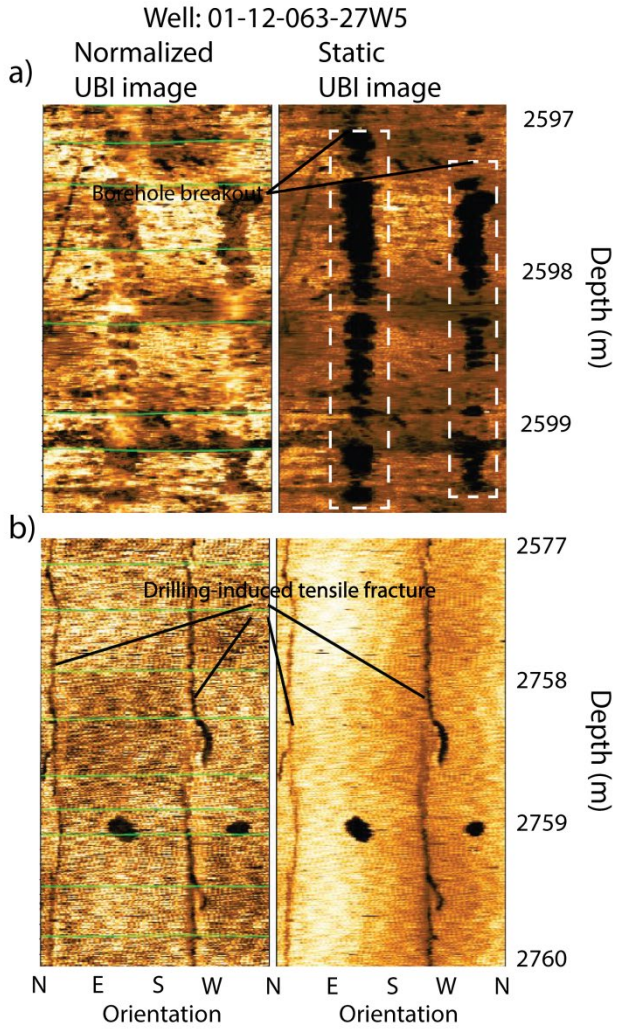

Figure 11. Sample Ultrasonic Borehole Imager (UBI™) wellbore images with identifiable a) borehole breakouts (BOs), and b) drilling-induced tensile fractures (DITFs).

Note that the example given in Figure 11 is one of the higher quality logs. There are noticeable cases where breakouts are often mimicked by other phenomena, so care must be taken in the interpretation of these features. Damage to the borehole wall during drilling or reaming can often be mistakenly interpreted. Also, natural fractures or large cavities may produce responses similar to those expected from BOs and DITFs. To ensure the accuracy of the BO and DITF identification, we employed the following assessment criteria:

1) The identified BOs and DITFs should be roughly aligned with the expected stress orientation of ~N45°E in this part of Alberta, compiled in the World Stress Map (Heidbach et al., 2016) with recent additions (Reiter et al., 2014).
2) The BO and DITF directions should be consistent along the length of the borehole. A certain amount of variation in the stress orientation is expected, although the stress orientation should generally be roughly consistent in any given location because Alberta is generally considered tectonically stable.
3) The orientations of BOs and DITFs in a given location must be approximately 90° apart from each other because they represent the directions of S_h and S_H, which must be 90° apart to fulfill the required symmetry of the stress tensor.
4) Only pairs of BOs or DITFs appearing along the same spring line through the borehole (i.e., 180° apart) are acceptable.

4 Results

The data analyzed in this study are extracted from compilations of borehole measurements from the Duvernay Formation in Alberta that include

1) more than 600 density logs integrated into profiles of S_V for the Kaybob assessment area;
2) 38 pressure-decline curves reanalyzed here for more confident P_{FC} and S_h constraints; another six reported results from tests carried out by industry had insufficient data for analysis to provide measures of the magnitude of S_h but were still included in this compilation;
3) 16 pressure-decline tests analyzed here and 26 tests carried out by industry, the latter with insufficient data to conduct analysis and verification for the reported P_P; and
4) 19 borehole-image logs that give indications of horizontal-stress directions and interpreted BO azimuthal widths to constrain the magnitude of S_H.

4.1 Vertical-Stress (S_V) Gradient

Figure 12 shows the computed vertical-stress gradient for the Duvernay Formation top in the Kaybob assessment area. The oil and gas industry often refers to the stress magnitude to depth ratio as the 'stress/pressure gradient.' Although such a gradient does not necessarily reflect the actual slope or derivative of the vertical-stress profile, it is potentially equal to the average $\delta S(d) / \delta d$ (S is stress and d is depth) from the surface to the measurement point if surface stress is assumed to be zero. Despite being debatable and possibly misleading, this 'gradient' provides a means of comparing stress measurements at different depths and shows the horizontal variation of the stress magnitudes. For illustration purposes, the average vertical-stress gradient appears to be ~23–26 kPa/m in the Duvernay Formation.

4.2 Minimum Horizontal-Stress (S_h) Gradient

In this study, the 38 DFITs conducted at or near the Duvernay Formation were collected and analyzed. Another six DFITs reported by industry but lacking actual pressure data were also included in this study. Figure 13 shows the closure gradients (S_h to depth ratio) estimated from these tests for the Duvernay Formation top in the Kaybob assessment area, with the S_h determined through the *G-function* approach. Ordinary kriging was performed on the data to assess S_h magnitudes where the measurement point is absent. The average gradient of S_h is estimated to be 17–21 kPa/m. The northeastern part of the study area has noticeably lower S_h values than the southwestern part. The S_h gradient is observed to be noticeably lower than that of S_V (~ 23–26 kPa/m). This seems to be in agreement with the focal-mechanisms analysis from nearby earthquakes, which indicates that the seismogenic faults in the region are strike slip (Schultz et al., 2017). Fracture-closure pressures recorded through the various analysis methods described in Section 3.2 are also provided in the accompanying dataset.

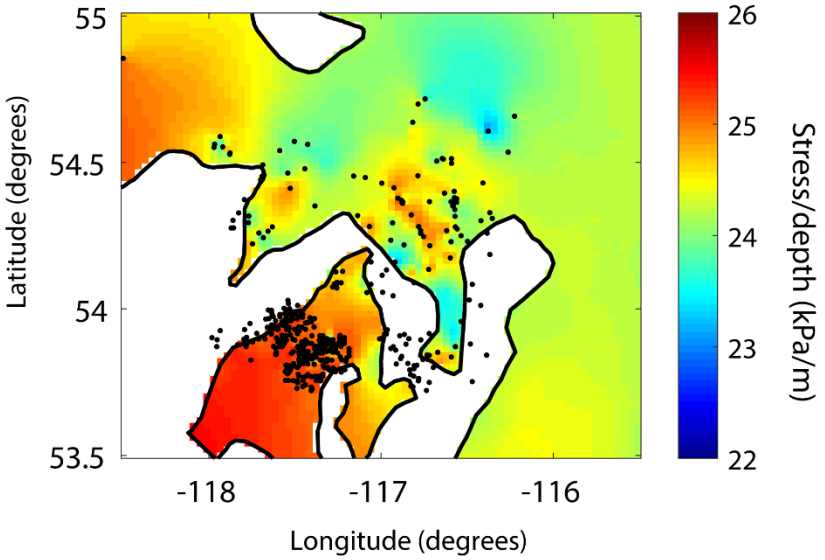

Figure 12. Estimated vertical-stress gradient at the top of Duvernay Formation in the study area. Black lines mark the zero-thickness edge between the Duvernay Formation and the coeval Leduc reefs, and black dots indicate locations of the wells from which density-log information at 2000 m depth is available for extraction.

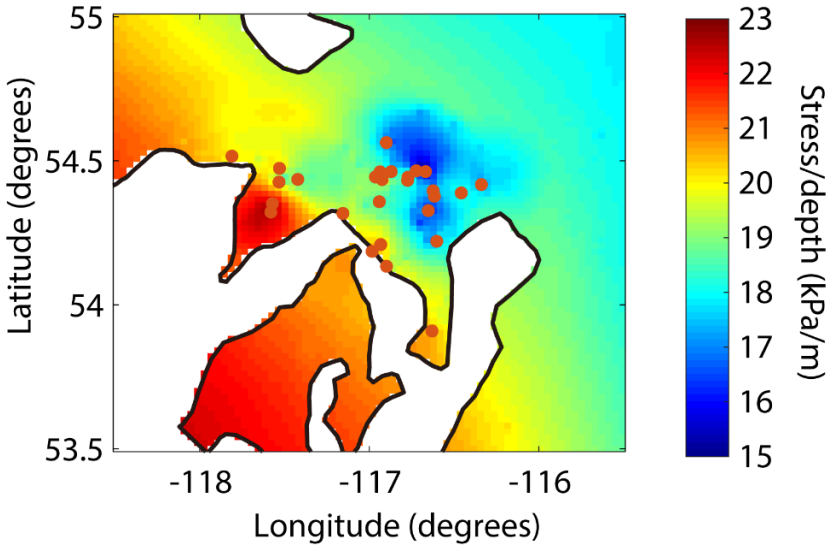

Figure 13. Estimated fracture-closure gradient at the top of the Duvernay Formation in the study area. Black lines mark the boundary between the Duvernay Formation and the coeval Leduc reefs, and red dots indicate the locations of DFITs reported within the study area.

4.3 Formation Pore-Pressure (P_P) Gradient

Formation pore pressures were analyzed by combining the results from DFITs, static-gradient tests, flow tests, and buildup tests. Static-gradient survey measurements were extracted from industry reports. Figure 14 shows the averaged pore-pressure gradients (pressure to depth ratio) in the study area computed from 39 of the collected pore-pressure measurements using the various techniques described in Section 3.3. The pore-pressure measurements for each well test were estimated using the averaged values determined from the methods described in Section 3.3, assuming that the final flow regime in the

wellbore was radial. Average values from the Nolte and Soliman-Craig methods are taken here as the formation-fluid pressures measured through DFITs. The average pore-pressure gradient appears to be ~16 kPa/m, which indicates that the Duvernay Formation in this area is considerably overpressured; this result agrees with previous observations reported by Davis and Karlen (2013) and Fox and Soltanzadeh (2015). It is also noteworthy that the pore-pressure distribution in this study area follows similar trends observed on the S_h map, namely that the northeastern part of the area is less overpressured than the southwestern part. This may be attributed to the higher pore pressure that results from the higher compaction and low permeability of the Duvernay shale.

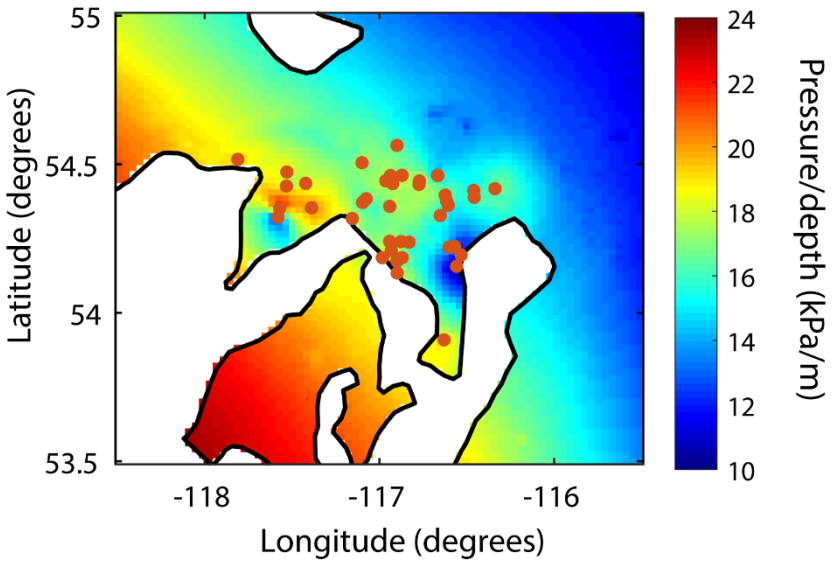

Figure 14. Estimated formation pore pressure at the top of Duvernay Formation in the study region, determined from 39 formation pore-pressure measurements. Black lines mark the boundary between the Duvernay Formation and juxtaposed Leduc reefs, and red dots indicate the locations of pressure surveys.

A small number of wells show significantly lower pore pressure than their neighbours. Re-examination of the well-testing results shows no evidence of erroneous data.

4.4 Orientations of Maximum Horizontal Compression (S_H)

New stress-orientation measurements were also added to the existing stress database from the WSM. Figure 15 shows the new measurements extracted from the wellbore images. The wellbore images analyzed in this study are deeper (mostly 2000–3500 m) than those on the WSM (often shallower than 1000 m). The maximum principal stresses are oriented at 30–50°. We did not observe significant discrepancies between our measurements and those reported on the WSM.

4.5 Constraints on Magnitude of Maximum Horizontal Stress (S_H)

A limited number of S_H values have been constrained using the recorded width of BOs collected during this study in conjunction with Equation 23. Figure 16 shows a vertical profile of our measurements from the study area. The S_H is noticeably higher than S_V at the same depths, whereas S_h is lower than S_V. The pore pressure, on the other hand, is only slightly lower than the S_h. The magnitude of S_H is constrained at ~100 MPa at 2800 m depth and rises to ~130 MPa at 4000 m. The gradient of S_H is estimated to be 33 ±2 kPa/m. The unconfined compressive strength (UCS) of the formation rocks used in Equation 23 is

assumed to be 100 MPa in this study. The intent of this report is to provide very preliminary constraints for S_H. Refinement of the constraints on S_H will be explored in future research.

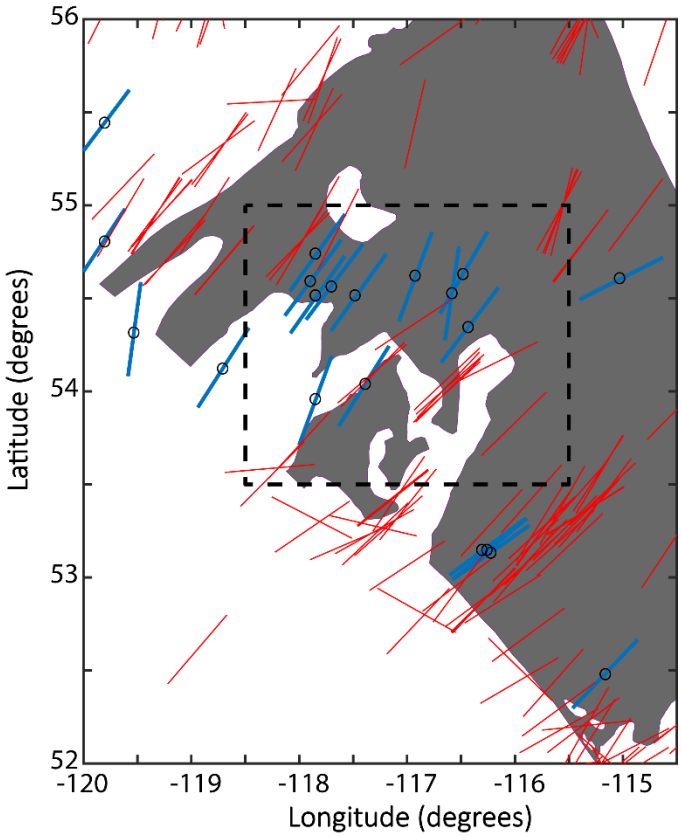

Figure 15. Updated stress-orientation map for the study area and immediate surroundings. Blue lines show the newly added stress-orientation measurements and red lines represent the measurements reported from the existing WSM database. Black circles show the locations of the wellbores from which the image logs were retrieved. Dashed black outline marks the region where P_P and S_h are mapped in Figures 13 and 14.

5 Conclusions

In this study, we describe the methods used in analyzing various datasets of regional in situ stress states and orientations.

Results from diagnostic fluid-injection tests carried out by the oil and gas industry were collected and analyzed in this study to constrain the minimum horizontal stress (S_h) in the Duvernay Formation near Fox Creek, Alberta. The gradient (stress to depth ratio) averages between 19 and 20 kPa/m, with highest and lowest values of 22 and 17 kPa/m, respectively. Results of static and transient well-pressure tests were collected and analyzed to study the formation pore pressures of the region. Although outliers exist, we observed that the majority of the study area is overpressured, with the pore-pressure gradient varying between ~13 and 20 kPa/m and averaging ~16 kPa/m. We also observed that the pore-pressure gradient is positively correlated with the S_h gradient. The vertical stress for the region was computed from collected density logs. The vertical-stress gradient (~25 kPa/m) appears to be higher than the minimum horizontal stress, confirming the strike-slip stress regime observed from induced-seismic focal mechanisms (Schultz et al., 2017).

The stress orientation has been updated from new image logs on the basis of the existing World Stress Map (WSM) measurements, with most of the records for Alberta originating from Haug and Bell (2016). Borehole breakout widths from high-quality image logs are recorded in our dataset as well. The interpretation of the image logs collected for this study shows high consistency with the WSM observations: the azimuth of S_H appears to be between 35 and 42° throughout the area of Fox Creek in west-central Alberta.

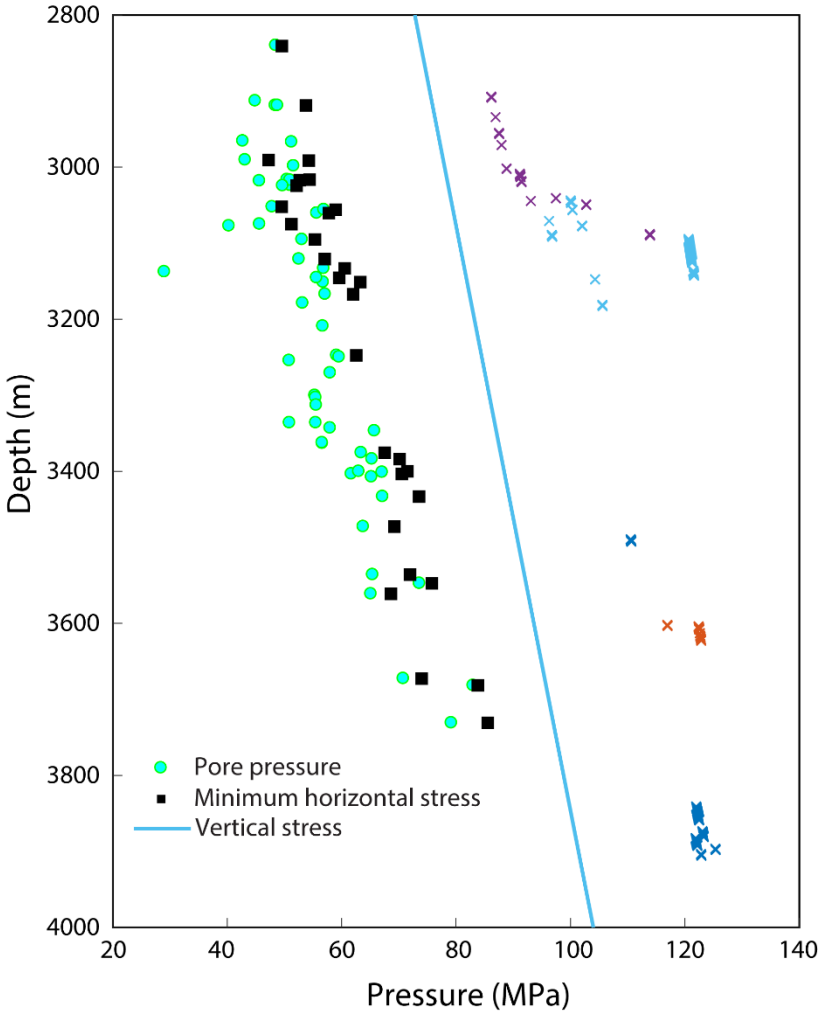

Figure 16. Vertical profile for the maximum horizontal stress (S_H) magnitudes constrained in this study. Cyan dots represent our pore-pressure measurements, black squares show the S_h measurements, blue line indicates the estimated S_V, and crosses with various colours are the S_H measurements from different wellbores.

6 References

Ahmed, T. and McKinney, P. (2011): Advanced Reservoir Engineering (revised); Elsevier, 424 p.

Anderson, E.M. (1905): The dynamics of faulting; Transactions of the Edinburgh Geological Society, v. 8, no. 3, p. 387–402.

Atkinson, G.M., Eaton, D.W., Ghofrani, H., Walker, D., Cheadle, B., Schultz, R., Shcherbakov, R., Tiampo, K., Gu, J., Harrington, R.M. and Liu, Y. (2016): Hydraulic fracturing and seismicity in the Western Canada Sedimentary Basin; Seismological Research Letters, v. 87, no. 3, p. 631–647.

Babcock, E.A. (1978): Measurement of subsurface fractures from dipmeter logs; AAPG Bulletin, v. 62, no. 7, p. 1111–1126.

Barree, R.D., Barree, V.L. and Craig, D. (2009): Holistic fracture diagnostics: consistent interpretation of prefrac injection tests using multiple analysis methods; SPE Production & Operations, v. 24, no. 3, p. 396–406.

Barton, C.A., Zoback, M.D. and Burns, K.L. (1988): In-situ stress orientation and magnitude at the Fenton geothermal site, New Mexico, determined from wellbore breakouts; Geophysical Research Letters, v. 15, no. 5, p. 467–470.

Bell, J.S. and Babcock, E.A. (1986): The stress regime of the Western Canadian Basin and implications for hydrocarbon production; Bulletin of Canadian Petroleum Geology, v. 34, no. 3, p. 364–378.

Bell, J.S. and Bachu, S. (2003): In situ stress magnitude and orientation estimates for Cretaceous coal-bearing strata beneath the plains area of central and southern Alberta; Bulletin of Canadian Petroleum Geology, v. 51, no. 1, p. 1–28.

Bell, J.S. and Gough, D.I. (1979): Northeast-southwest compressive stress in Alberta evidence from oil wells; Earth and Planetary Science Letters, v. 45, no. 2, p. 475–482.

Bell, J.S. and Grasby, S.E. (2012): The stress regime of the Western Canadian Sedimentary Basin; Geofluids, v. 12, no. 2, p. 150–165.

Bell, J.S., Price, P.R. and McLellan, P.J. (1994): In-situ stress in the Western Canada Sedimentary Basin; Chapter 29 *in* Geological Atlas of the Western Canada Sedimentary Basin, G.D. Mossop and I. Shetsen (ed.), Canadian Society of Petroleum Geologists, Calgary, Alberta and Alberta Research Council, Edmonton, Alberta, p. 439–446.

Castillo, J.L. (1987): Modified fracture pressure decline analysis including pressure-dependent leakoff; Low-Permeability Reservoirs Symposium, Denver, Colorado, May 18–19, 1987, Paper SPE 16417, https://doi.org/10.2118/16417-MS.

Cinco-Ley, H. (1981): Transient pressure analysis for fractured wells; Journal of Petroleum Technology, v. 33, no. 9, p. 1–749.

Craig, D.P., Barree, R.D., Warpinski, N.R. and Blasingame, T.A. (2017): Fracture closure stress: re-examining field and laboratory experiments of fracture closure using modern interpretation methodologies; Society of Petroleum Engineers, Annual Technical Conference and Exhibition, October 9-11, San Antonio, Texas, Paper SPE-187038-MS, https://doi.org/10.2118/187038-MS.

Davis, M. and Karlen, G. (2013): A regional assessment of the Duvernay Formation; a world-class liquids-rich shale play; extended abstract of presentation at CSPG/CSEG/CWLS GeoConvention 2013, (Integration: Geoscience Engineering Partnership), Calgary, Alberta, May 6-12, 2013, Search and Discovery Article #10638 (2014), URL <http://www.searchanddiscovery.com/pdfz/documents/2014/10638davis/ndx_davis.pdf.html> [August 2018].

Detournay, E., Cheng, A.D., Roegiers, J.C. and McLennan, J.D. (1989): Poroelasticity considerations in in situ stress determination by hydraulic fracturing; International Journal of Rock Mechanics and Mining Sciences & Geomechanics Abstracts, v. 26, no. 6, p. 507–513.

Doe, T., Ingevald, K., Strindell, L., Haimson, B. and Carlsson, H. (1981): Hydraulic fracturing and overcoring stress measurements in a deep borehole at the Stripa test mine, Sweden; American Rock Mechanics Association, 22nd U.S. Symposium on Rock Mechanics (USRMS), June 29–July 2, 1981, Cambridge, Massachusetts, Paper ARMA-81-0373, URL <https://www.onepetro.org/conference-paper/ARMA-81-0373> [August 2018].

Ellis, D.V. and Singer, J.M. (2007): Well Logging for Earth Scientists (Second Edition); Springer, Dordrecht, 692 p., https://doi.org/10.1007/978-1-4020-4602-5.

Fordjor, C.K., Bell, J.S. and Gough, D.I. (1983): Breakouts in Alberta and stress in the North American plate; Canadian Journal of Earth Sciences, v. 20, no. 9, p. 1445–1455.

Fox, A.D. and Soltanzadeh, M. (2015): A regional geomechanical study of the Duvernay Formation in Alberta, Canada; paper presented at GeoConvention 2015, *Geoscience: New Horizons*, May 4–8, 2015, Calgary, Alberta.

Gough, D.I. and Bell, J.S. (1981): Stress orientations from oil well fractures in Alberta and Texas; Canadian Journal of Earth Sciences, v. 18, p. 638–645.

Gough, D.I., and Bell, J.S. (1982): Stress orientation from borehole wall fractures with examples from Colorado, east Texas, and northern Canada; Canadian Journal of Earth Sciences, v. 19, p. 1358–1370.

Green, D.G. and Mountjoy, E.W. (2005): Fault and conduit controlled burial dolomitization of the Devonian west-central Alberta Deep Basin; Bulletin of Canadian Petroleum Geology, v. 53., no. 2, p. 101–129.

Haimson, B.C. and Rummel, F. (1982): Hydrofracturing stress measurements in the Iceland research drilling project drill hole at Reydarfjordur, Iceland; Journal of Geophysical Research: Solid Earth, v. 87, no. B8, p. 6631–6649.

Haug, K. and Bell, J.S. (2016): Compilation of in situ stress data from Alberta and northeastern British Columbia (tabular data, tab delimited); Alberta Energy Regulator, AER/AGS Digital Data 2016-0040, URL <https://ags.aer.ca/publications/DIG-2016-0040.html> [August 2018].

Heidbach, O., Rajabi, M., Reiter, K., Ziegler, M. and WSM Team (2016): World Stress Map Database Release 2016; GFZ Data Services, http://doi.org/10.5880/WSM.2016.001.

Henton, J.A., Craymer, M.R., Dragert, H., Mazzotti, S., Ferland, R. and Forbes, D.L. (2006): Crustal motion and deformation monitoring of the Canadian landmass; Geomatica, v. 60, no. 2, p. 173–191.

Horner, D.R. (1951): Pressure build-up in wells; 3rd World Petroleum Congress, May 28–June 6, 1951, The Hague, Netherlands, Paper WPC-4135, URL <https://www.onepetro.org/conference-paper/WPC-4135> [August 2018].

Howard, G.C. and Fast, C.R. (1957): Optimum fluid characteristics for fracture extension; American Petroleum Institute, *Drilling and Production Practice*, January 1, 1957, New York, New York, Paper API-57-261, https://www.onepetro.org/conference-paper/API-57-261 [August 2018].

Morin, M.L. (2017): Natural and drilling induced fractures in the Grosmont Formation, Alberta: implications for the state of stress; M.Sc. thesis, University of Alberta, Edmonton, Alberta, 108 p.

Nolte, K.G. (1979): Determination of fracture parameters from fracturing pressure decline; Society of Petroleum Engineers, Annual Technical Conference and Exhibition, September 23–26, Las Vegas, Nevada, Paper SPE-8341-MS, https://doi.org/10.2118/8341-MS.

Nolte, K.G. (1986): A general analysis of fracturing pressure decline with application to three models; SPE Formation Evaluation, v. 1, no. 6, p. 571–583.

Pawley, S., Schultz, R., Playter, T., Corlett, H., Shipman, T., Lyster, S. and Hauck, T. (2018): The geological susceptibility of induced earthquakes in the Duvernay play; Geophysical Research Letters, v. 45, no. 4, p. 1786–1793.

Plumb, R.A., Evans, K.F. and Engelder, T. (1991): Geophysical log responses and their correlation with bed-to-bed stress contrasts in Paleozoic rocks, Appalachian Plateau, New York; Journal of Geophysical Research: Solid Earth, v. 96, no. B9, p. 14509–14528.

Preston, A., Garner, G., Beavis, K., Sadiq, O. and Stricker, S. (2016): Duvernay reserves and resources report: a comprehensive analysis of Alberta's foremost liquids-rich shale resource; Alberta Energy Regulator, AER report, 83 p., <https://www.aer.ca/documents/reports/DuvernayReserves_2016.pdf> [August 2018].

Reiter, K., Heidbach, O., Schmitt, D., Haug, K., Ziegler, M. and Moeck, I. (2014): A revised crustal stress orientation database for Canada; Tectonophysics, v. 636, p. 111–124, http://dx.doi.org/10.1016/j.tecto.2014.08.006.

Rokosh, C.D., Lyster, S., Anderson, S.D.A., Beaton, A.P., Berhane, H., Brazzoni, T., Chen, D., Cheng, Y., Mack, T., Pana, C. and Pawlowicz, J.G. (2012): Summary of Alberta's shale- and siltstone-hosted hydrocarbon resource potential; Energy Resources Conservation Board, ERCB/AGS Open File Report 2012-06, 327 p. URL <https://ags.aer.ca/publications/OFR_2012_06.html>[August 2018]

Schmitt, D.R. (2014): Basic geomechanics for induced seismicity: a tutorial, CSEG Recorder, v. 39, no. 11, p. 24–29.

Schmitt, D.R. and Haimson, B.C. (2017): Hydraulic fracturing stress measurements in deep holes; Chapter 6 *in* Rock Mechanics and Engineering, Volume 1: Principles, X-T. Feng (ed.), CRC Press, p. 183–225.

Schmitt, D.R., Currie, C.A. and Zhang, L. (2012): Crustal stress determination from boreholes and rock cores: fundamental principles; Tectonophysics, v. 580, p. 1–26, http://dx.doi.org/10.1016/j.tecto.2012.08.029.

Schultz, R., Wang, R., Gu, Y.J., Haug, K. and Atkinson, G. (2017): A seismological overview of the induced earthquakes in the Duvernay play near Fox Creek, Alberta; Journal of Geophysical Research: Solid Earth, v. 122, no. 1, p. 492–505.

Shen, L., Schmitt, D.R. and Haug., K (2018): In-situ stress measurements for the Duvernay formation, Alberta (tabular data, tab-delimited format); Alberta Energy Regulator / Alberta Geological Survey, AER/AGS Digital Data 2018-0013, URL <https://ags.aer.ca/publications/DIG_2018_0013.html> [October 2018].

Soliman, M.Y., Craig, D.P., Bartko, K.M., Rahim, Z. and Adams, D.M. (2005): Post-closure analysis to determine formation permeability, reservoir pressure, residual fracture properties; Society of Petroleum Engineers, Middle East Oil and Gas Show and Conference, March 12–15, 2005, Kingdom of Bahrain, Paper SPE-93419-MS, https://doi.org/10.2118/93419-MS.

Wang, R., Gu, Y.J., Schultz, R., Kim, A. and Atkinson, G. (2016): Source analysis of a potential hydraulic-fracturing-induced earthquake near Fox Creek, Alberta; Geophysical Research Letters, v. 43, no. 2, p. 564–573.

Wang, R., Gu, Y.J., Schultz, R., Zhang, M. and Kim, A. (2017): Source characteristics and geological implications of the January 2016 induced earthquake swarm near Crooked Lake, Alberta; Geophysical Journal International, v. 210, no. 2, p. 979–988.

Woodland, D.C. and Bell, J.S. (1989): In situ stress magnitudes from mini-frac records in western Canada; Journal of Canadian Petroleum Technology, v. 28, no. 5, 11 p., https://doi.org/10.2118/89-05-01.

Zanganeh, B., MacKay, M.K., Clarkson, C.R. and Jones, J.R. (2018): DFIT analysis in low leakoff formations: a Duvernay case study; Society of Petroleum Engineers, SPE Canada Unconventional Resources Conference, March 13–14, 2018, Calgary, Alberta, Paper SPE-189826-MS, https://doi.org/10.2118/189826-MS.

Zoback, M.D. (2007): Reservoir Geomechanics; Cambridge University Press, Cambridge, United Kingdom, 489 p.

Zoback, M.D. and Zoback, M.L. (1991): Tectonic stress field of North America and relative plate motions; Neotectonics of North America, v. 1, p. 339–366.